Organic Geochemistry 212 (2026) 105092

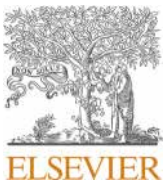

Contents lists available at ScienceDirect

Organic Geochemistry

journal homepage: www.elsevier.com/locate/orggeochem

Plant-wax *n*-alkanes from the central Congo Basin as palaeo-environmental and -climatic proxies

Mélanie Guardiola [a,*], Gaël U.D. Bouka [b], Carolia Abaye [b], Johanna Menges [c], Frauke Rostek [a], Guillaume Leduc [a], Edouard Bard [a], Enno Schefuß [c], Yannick Garcin [a,*]

[a] Aix-Marseille University, CNRS, IRD, Collège de France, INRAE, CEREGE, Aix-en-Provence, France
[b] Université Marien Ngouabi, Faculté des Sciences et Techniques, Laboratoire de Biodiversité, Gestion des Ecosystèmes et de l'Environnement, Brazzaville, Republic of the Congo
[c] MARUM – Center for Marine Environmental Sciences, University of Bremen, Bremen, Germany

ARTICLE INFO

Associate Editor: Nikolai Pedentchouk

Keywords:
Central Congo Basin
Peatlands
Plant wax
n-Alkane
Carbon isotopes
Hydrogen isotopes
Palaeo-environment
Palaeo-climate

ABSTRACT

The central Congo Basin is home to the world's largest tropical peatland complex and is covered with swamp forest. In the face of climate change and future human activities in the region, it is important to understand the factors that determine the nature and dynamics of the peatland vegetation cover. One way to gain insight into these factors is to reconstruct the history of the central Congo Basin peatlands. Analysing lipid biomarkers extracted from peat cores such as plant wax *n*-alkanes enables past environmental and climatic conditions to be reconstructed. However, there is currently no information on how the production of plant waxes by different plant species influences the abundance and isotopic composition of *n*-alkanes in peat and other archives in the Congo Basin. In this study we analysed plant wax *n*-alkane abundances, $\delta^{13}C$ and δD values according to photosynthetic pathways (C_3 vs. C_4), angiosperm subclasses (dicotyledons vs. monocotyledons), and source water δD values in the dominant plant types (trees, shrubs, and herbs) in the peatland area of the Cuvette Department in the Republic of the Congo. Our dataset enables the definition of a new *n*-alkane distribution index, named GRIND, that distinguishes between C_3 (mostly dicotyledons) and C_4 (monocotyledons) plants as follows: (n-C_{27} + n-C_{33} + n-C_{35})/(n-C_{25} + n-C_{27} + n-C_{29} + n-C_{31} + n-C_{33} + n-C_{35}). This index may therefore be used to analyse Central African peat deposits and derive the relative abundance of C_3 and C_4 plant waxes in the past, independently of $\delta^{13}C$ measurements. Furthermore, $\delta^{13}C$ values from the central Congo Basin and other African sites suggest that environments with high relative humidity (> 80%) are characterised by very negative $\delta^{13}C$ values (i.e., < –37‰) of n-C_{29} and n-C_{31} alkanes. This observation highlights the potential of *n*-alkane $\delta^{13}C$ in deriving climatic information under high relative humidity conditions in Central African lowlands, and contribute to palaeo-climatic reconstructions. Finally, the δD values of n-C_{29} and n-C_{31} alkanes demonstrate that, despite contrasting apparent fractionation values associated with photosynthetic pathways and plant functional types — which can be accounted for using $\delta^{13}C$ and pollen data in sedimentary deposits — they reliably reflect the δD of environmental water. This confirms that plant wax *n*-alkane δD values are effective tools for reconstructing palaeo-climatic changes in equatorial regions.

1. Introduction

Peatlands are defined as carbon-rich ecosystems that play an important role in the global carbon cycle (see Page et al., 2011). The peatlands of the central Congo Basin (CCB) have recently been identified as the world's largest tropical peatland complex (Dargie et al., 2017), encompassing an estimated area of 167,600 km^2, representing 36% of the global tropical peatland area (Crezee et al., 2022). The below-ground carbon density of peat in the CCB is estimated at 1,712 ±634 MgC ha^{-1} (Crezee et al., 2022), which is nine times higher than the average carbon density stored in the above-ground biomass of living trees in African tropical forests (Lewis et al., 2013). Therefore, it is crucial to understand how these peatlands formed and the conditions under which they continue to function as a carbon sink.

For several decades, lipid biomarkers from terrestrial plants have been widely used as palaeo-environmental and palaeo-climatic proxies,

* Corresponding authors.
E-mail addresses: melani.guardiola@gmail.com (M. Guardiola), garcin@cerege.fr (Y. Garcin).

https://doi.org/10.1016/j.orggeochem.2025.105092
Received 29 July 2025; Received in revised form 21 October 2025; Accepted 16 November 2025
Available online 17 November 2025

particularly where other data sources, such as pollen or macrofossils, are poorly preserved. Recently, the first studies relying on lipid biomarkers in the CCB have also been published (Garcin et al., 2022; Hawthorne et al., 2023; Menges et al., 2025). Long-chain *n*-alkanes derived from plant epicuticular waxes are the most common type used (Meyers, 2003; Schefuß et al., 2003; Seki et al., 2010; Diefendorf and Freimuth, 2017). These long-chain *n*-alkanes contain only carbon and hydrogen atoms, belong to the saturated linear hydrocarbon family, are resistant to degradation (Bush and McInerney, 2013), and are also ubiquitous in ancient sedimentary archives (Pancost and Boot, 2004). Consequently, they have been identified as robust biomarkers capable of determining biological origin and environmental conditions (Eglinton and Hamilton, 1967; Meyers, 1997).

In sedimentary archives, the distribution of *n*-alkanes is usually characterised by a clear preference for odd over even carbon-numbered homologues. This is reflected in high Carbon Preference Index (CPI) values, which are indicative of the presence of recent undegraded terrestrial plant matter (Bray and Evans, 1961). Average Chain Length (ACL) also provides insights into dominant vegetation types (Poynter et al., 1989), with monocotyledons (monocots) exhibiting higher ACL values than dicotyledons (dicots; Cranwell, 1984; Meyers, 2003; Duan and He, 2011; Wang et al., 2018). Total *n*-alkane abundance is also a valuable proxy for assessing plant primary productivity and/or quantifying the contribution of plant-derived organic matter to terrestrial and aquatic depositional environments (Meyers, 2003; Diefendorf and Freimuth, 2017).

The stable carbon isotope values of *n*-alkanes ($\delta^{13}C_{n\text{-alkane}}$) are frequently used to reconstruct vegetation types in tropical regions (C_3 vegetation being typically tree-dominated while C_4 vegetation being typically graminoid-dominated; Feakins et al., 2005; Castañeda et al., 2009; Collins et al., 2011). This is related to the significant influence that the carbon fixation pathway (C_3 vs. C_4) exerts on the $\delta^{13}C_{n\text{-alkane}}$ values of higher plants during the process of photosynthesis (Chikaraishi and Naraoka, 2003; Collister et al., 1994; Garcin et al., 2014; Rieley et al., 1991).

The stable hydrogen isotope values of *n*-alkanes ($\delta D_{n\text{-alkane}}$) are frequently used in hydroclimatic reconstructions on a global scale, including tropical African regions, where they have helped to track changes in past precipitation patterns, including the amount, the wet season precipitation, and the source of precipitation (Schefuß et al., 2005; Shanahan et al., 2015; Tierney et al., 2017; Ladd et al., 2021; Garcin et al., 2022; Zhao et al., 2024). Such reconstructions are possible because the $\delta D_{n\text{-alkane}}$ values of long chain homologues are generally unaffected by isotopic changes caused by the selective decomposition of labile compounds. This is because the hydrogen atoms are carbon-bound and typically non-exchangeable under low-temperature, near-surface conditions (Schimmelmann et al., 1999). However, over longer geological timescales and at elevated burial temperatures in the presence of mineral catalyst, partial hydrogen exchange may occur (Sessions, 2016). Furthermore, since plants use environmental water (i.e., soil water, which is predominantly related to meteoric water) during biosynthesis, $\delta D_{n\text{-alkane}}$ can capture climatic variations that control the isotopic fractionation of meteoric water (Epstein et al., 2001; Garcin et al., 2012; Sachse et al., 2006). However, it has been demonstrated that divergent vegetation types (e.g., those associated with disparate C_3 or C_4 photosynthetic cycles) may lead to shifts in $\delta D_{n\text{-alkane}}$ values that are unrelated to climatic variability (Griepentrog et al., 2019). Indeed, it has been shown that physiological differences in plants can result in different transpiration strategies in response to water stress, leading to different apparent isotopic fractionations between source water hydrogen and lipid hydrogen (Sachse et al., 2012). $\delta^{13}C_{n\text{-alkane}}$ values are often used to correct for this vegetation effect (Collins et al., 2013; Wang et al., 2013; Shanahan et al., 2015; Tierney et al., 2017; Garcin et al., 2018).

Sedimentary archives accumulate a mixture of waxes from different plants over time, thereby integrating a mosaic of different biomes and vegetation cover types. For instance, the composition of leaf wax *n*-alkanes can vary according to canopy position and leaf ontogeny (Dyson and Herbin, 1968; Lockheart et al., 1997; Feakins and Sessions, 2010; Kahmen et al., 2011), further obscuring the sedimentary signal. In order to interpret the results of the analysis of sedimentary $\delta^{13}C_{n\text{-alkane}}$ and $\delta D_{n\text{-alkane}}$, it is hence necessary to understand the processes involved in the production of plant lipids in living plants from the studied region. Such calibration efforts have been conducted in various regions worldwide (e.g., Sachse et al., 2006; Pedentchouk et al., 2008; Hoffmann et al., 2013; Tipple and Pagani, 2013), including in Africa (e.g., Vogts et al., 2009; Garcin et al., 2012, 2014; Gensel et al., 2022; Tweedy et al., 2025). Despite the fact that certain studies have used plant lipids to reconstruct palaeo-environments and -climates in the CCB (Garcin et al., 2022; Hawthorne et al., 2023; Menges et al., 2025), there are currently no direct measurements available on the distribution and stable isotope compositions of carbon and hydrogen in plant waxes from living plants of the CCB (Pancost, 2024).

In this study, we analysed the distribution and abundance of *n*-alkanes, along with their $\delta^{13}C_{n\text{-alkane}}$ and $\delta D_{n\text{-alkane}}$ values, in the leaves of living plants collected in the CCB (see Figs. 1 and 2). We also measured the isotopic composition of environmental surface water (e.g., river water and peat surface water) to identify the hydrogen isotopic composition of the source water of the plants and, by extension, the stable hydrogen isotope fractionation between water and lipids. We evaluated the $\delta^{13}C_{n\text{-alkane}}$ and $\delta D_{n\text{-alkane}}$ values in relation to photosynthetic pathway (C_3 vs. C_4), angiosperm subclasses (dicots vs. monocots), and the δD values of environmental surface waters. The present study provides an interpretative framework for detailed palaeo-environmental and palaeo-climatic reconstructions in the CCB and beyond.

2. Study site

During a field campaign, samples of terrestrial and aquatic plants and environmental surface waters were collected from sites representative of the tropical peatlands of the CCB, as well as from the Congo River tributaries (see Fig. 1 for details). The present study was conducted within a catchment area in the northern part of the Republic of the Congo (Fig. 1), specifically in the districts of Mossaka (Cuvette Department) and Liranga (Likouala Department), both of which are located within the CCB. Sampling was conducted in areas largely comprising floodplains, up to 5 km inland from the main rivers, in the Kouyou, Likouala-Mossaka, Sangha and Congo river basins (from west to east).

2.1. Geological formation and soil type

The Congo River is located at an altitude of less than 400 m above sea level and traverses a variety of ecological zones, including swamps, grasslands, and equatorial forests. A significant proportion of these forests are subject to periodic or perennial flooding. The CCB is located within a shallow central depression (Laraque et al., 2009, 2020), which leads to a reduction in the velocity of river flow and a minimal degree of erosion due to the presence of negligible morphological gradients (~2 cm km^{-1}; Laraque et al., 2009). The topography of the CCB is characterised by a complex hydrographic network, comprising numerous flowing rivers and many shallow lakes. The soils of the CCB are composed of Quaternary alluvium (clay or sand), which are subject to constant reworking by the dense hydrographic network (Vennetier, 1966; Laidet, 1969; Boissezon and Gras, 1970). In the Mossaka area, the soils are predominantly fluvisols, hydromorphic soils with a thick humic horizon (Bocquier, 1960; Vennetier, 1966; Laidet, 1969). Soils are characterised by reduced fertility and low mineral content (Comptour, 2017). In the CCB, peatlands are on average 1.7 m thick, with a maximum thickness of 5.6 m (Dargie et al., 2017; Crezee et al., 2022). These peatlands have the capacity to store approximately 29 Pg of carbon, i.e., around one-third of the total carbon stored in tropical peatlands worldwide (Dargie et al., 2017; Crezee et al., 2022). Different

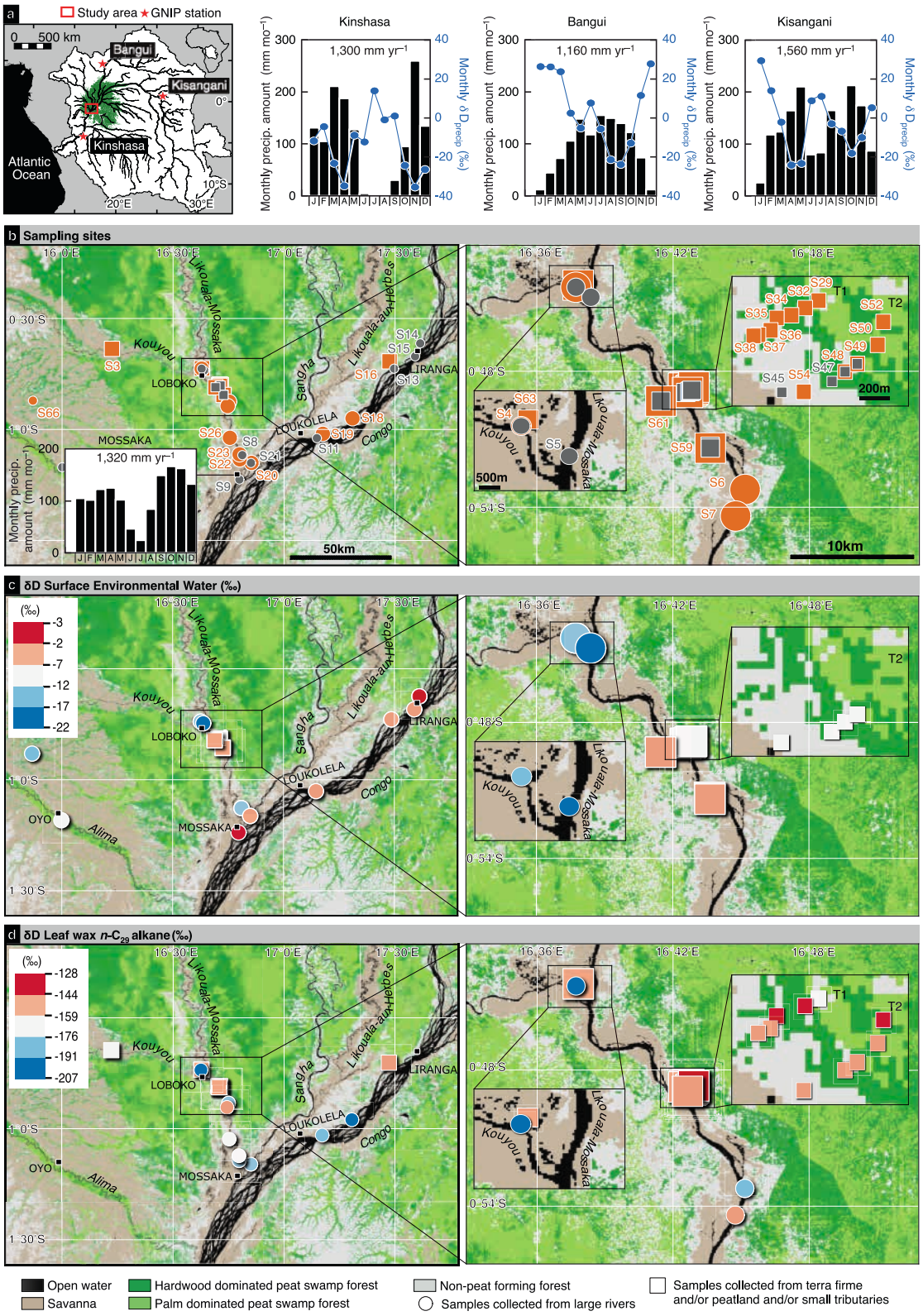

Fig. 1. Study sites within the central Congo Basin peatlands region. (a) Left: Map of the CCB peatlands (green) and the perimeter of the Congo Basin (black). Also shown is the study area (open red rectangle) and the three GNIP stations (Kinshasa, Bangui, and Kisangani) closest to the study area (red stars). Right: Diagrams of monthly δD_{precip} and precipitation amount for Kinshasa, Bangui, and Kisangani (IAEA/WMO, 2020). (b, c, d) Base map showing the spatial distribution of palm-dominated (light green) and hardwood-dominated (dark green) peat swamp forests in the study area (Crezee et al., 2022). (b) Sampling sites, with the locations of the water samples (grey) and the plant samples (orange). Also shown is the mean monthly precipitation for Mossaka (Comptour et al., 2020). (c) δD values of sampled environmental surface waters. (d) δD values of sampled leaf wax *n*-alkanes. (For interpretation of the references to colour in this figure legend, the reader is referred to the web version of this article.)

Fig. 2. Example of overlying vegetation within the CCB peatlands region. (a) Hardwood-dominated swamp, and (b) mixed palm-dominated and hardwood swamp overlying peat in the Likouala Department. (c) Flooded river banks, and (d) floating mats composed of *V. cuspidata*. (e) Savanna dominated by grasses and a few shrubs/trees, and (f) example of cultivated manioc (*Manihot esculenta* Crantz, *Manihot glaziovii* Müll, Arg), grown in villages along rivers. (credits Y. Garcin). (For interpretation of the references to colour in this figure legend, the reader is referred to the web version of this article.)

types of peat deposit can be distinguished according to their hydrological and geomorphological contexts (Dargie et al., 2017; Crezee et al., 2022). In the northern part of the Cuvette Centrale, primarily in the Republic of the Congo, ombrotrophic peat deposits form away from rivers, under the influence of rainfall, which maintains a high water table (Alsdorf et al., 2016; Datok et al., 2022). These deposits are distinguished by an absence of fluvial inputs, such as nutrients, and can form extensive, shallow domes (Davenport et al., 2020). In the Democratic Republic of the Congo, minerotrophic peat deposits also develop on floodplains that receive various inputs from rivers and groundwater, including water and nutrients (Lee et al., 2015; Crezee et al., 2022).

2.2. Climate and hydrology

The CCB is influenced by an equatorial climate (Köppen classification: tropical rainforest climate and tropical monsoon climate). The mean annual temperature in Mossaka is 26.2 °C, with an average annual rainfall of 1,320 mm (Comptour et al., 2020), and the relative humidity is consistently high (> 80%) throughout the year (Hersbach et al., 2020). Due to the migration of the Inter-Tropical Convergence Zone (ITCZ), the region's rainfall is bimodal, with four seasons in Mossaka as follows (Fig. 1b): (*i*) September to December is main rainy season; (*ii*) January and February correspond to the short dry season; (*iii*) March to May correspond to the short rainy season; and (*iv*) June to August the long dry season (Comptour, 2017).

The hydrological regime of the Congo River is characterised by two periods of low water and two periods of high water (Keddy et al., 2009; Laraque and Olivry, 1996; Wongchuig et al., 2023). The main rivers and their northern tributaries — the Congo, the Ubangui, the Sangha, and the Likouala-Mossaka — exhibit distinct hydrological regimes characterised as unimodal or bimodal distributions. The tributaries converging in Mossaka are impacted by a rise in their water levels delayed by one to

two months after the main rainy season peak, with a single flood period throughout the year (Comptour, 2017). This phenomenon leads to riverbeds exceeding their capacity, resulting in the inundation of floodplains. However, the precipitation patterns are observed to be erratic, and recurrent flooding is a common occurrence, thus exposing ecosystems to a multitude of hydro-climatic hazards, primarily flooding and, to a lesser extent, droughts (Samba et al., 2023). The southern tributaries that dominate the Congo River catchment follow an equatorial hydrological regime characterised by continuous flow throughout the year and two flood periods.

2.3. Vegetation

2.3.1. Spatial distribution and structure of vegetation formations in the Congo Basin

The Congo Basin is one of the largest areas of tropical moist forest that remains largely intact (Grantham et al., 2020; Shapiro et al., 2021); its ecological diversity is reflected in its wide range of vegetation formations, which have been extensively described and classified (Devred, 1958; Gérard, 1960; Trochain, 1957; Lebrun and Gilbert, 1954). The Congo Basin is organised around a central forest core that accounts for approximately 51% of the basin area, interspersed with non-forested internal areas (Shapiro et al., 2023). The central block is bordered by a forest margin which transitions into a fragmented corridor (27%), comprising isolated forest patches (Shapiro et al., 2023). Forest cover fragmentation increases progressively with distance from the forest core (Shapiro et al., 2023). In the CCB, forestry and agricultural activities are concentrated mainly on small *terra firme* forest plots located near villages (Dargie et al., 2019). The human impact on the forest landscape is organised in the form of a dispersed rural complex covering less than 8% of the area, and is primarily structured around shifting cultivation practices, and highlights the road network (Verhegghen et al., 2012; Molinario et al., 2015, 2017; Shapiro et al., 2023).

The Congo Basin is characterised by a hot and humid equatorial climate, which fosters the proliferation of dense tropical forests, a phenomenon that is archetypal of moist equatorial regions (Lebrun and Gilbert, 1954; Gérard, 1960). The central forests are classified as part of the Lower Guinea–Congo forests phytogeographical region (White, 1983), the central forests consists of a mature lowland dense mixed deciduous forests and in swamp forests (Fig. 2a; Mayaux et al., 2000; Verhegghen et al., 2012; Shapiro et al., 2023). The mature, evergreen tropical rainforest develops in better-drained interfluvial areas (Doumenge, 1990), and is characterised by a closed, homogeneous canopy that typically reaches heights of 35–45 m (Mayaux et al., 2000). The upper stratum consists of shade-tolerant species organised in a well-defined vertical structure with limited seasonal dynamics (Lebrun and Gilbert, 1954; Mayaux et al., 2000). The development of understory shrubs and grasses is rare, while epiphytes, such as members of the Arecaceae family, are favoured (Mayaux et al., 2000). The lower layers are composed of two distinct strata of regenerating individuals from the upper canopy (Lebrun and Gilbert, 1954). Swamp forests are characterised by the predominance of evergreen species, which have adapted to the condition of protracted flooding. These species exhibit distinctive traits such as stilt roots and pneumatophores (Evrard, 1968). These environments (Fig. 2b) are characterised by a high density of lianas and epiphytes, but relatively low floristic diversity. The homogeneous canopy can reach heights of up to 45 m and is often dominated by Caesalpiniaceae species such as *Guibourtia demeusei* (Harms) J. Léonard (Lebrun and Gilbert, 1954; Campbell, 2005).

Non-forested wetlands have also been identified in the CCB, particularly in the permanently flooded valleys of the Lower Likouala, the Likouala-aux-Herbes, and the Giri rivers (Hugues and Hugues, 1992; De Grandi et al., 2000; Campbell, 2005; Fig. 2c). These habitats are characterised by the predominance of rooted grasses growing in muddy substrates, including *Echinochloa pyramidalis* (Lam.) Hitchc. & Chase, *Leersia hexandra* Sw., *Oryza barthii* A. Chev., *Vossia cuspidata* (Roxb.) Griff. and large Carex species, some of which are capable of forming floating mats (Fig. 2d). To the west of the Cuvette Centrale, these grasslands form part of a mosaic landscape comprising steppes, savannas, peatlands, and swamps (Hugues and Hugues, 1992). Some areas, which are subject to seasonal drying, are also prone to fires. At the periphery of the central basin, semi-deciduous forests gradually become the most prevalent stable vegetation type (Devred, 1958). These forests host a mixture of deciduous and evergreen species, with canopies characterised by partial and asynchronous leaf loss (Mayaux et al., 2000). Beyond the main forest blocks, savannas comprise up to 40% of the Congo Basin (Laporte et al., 1998; Hansen et al., 2008). They are characterised by the presence of a continuous herbaceous layer interspersed with sparse trees and shrubs (Fig. 2e; see Mayaux et al. (2000)). Their structure is influenced by edaphic factors, climate, and fire regimes (Sankaran et al., 2005; Koechlin, 1961). In the northern region, the landscape is characterised by the prevalence of Guinean savannas, while in the southern region, Zambesian savannas are predominant, often interspersed with narrow gallery forests adjacent to rivers (Peeters, 1964; Mayaux et al., 2000) and isolated savanna patches (Koechlin, 1961). Plantations (Fig. 2f), including industrial ones (e.g., rubber, oil palm, and cotton) that were in part introduced during the colonial period, also contribute to the structuring of the landscape (Mayaux et al., 2000).

2.3.2. Vegetation formations of the study area (floodplains at the interface of the Likouala-Mossaka and the Congo rivers)

The paucity of information regarding the vegetation of the region is primarily attributable to the considerable size and inaccessibility of the CCB forested wetlands (Keddy et al., 2009). Nevertheless, an exhaustive list of swamp forest species has been compiled in the CCB (Hugues and Hugues, 1992; Moutsambote, 2012; Ifo et al., 2016), either in association with hydromorphic soils or swamp forest areas. Recent peatland mapping (Dargie et al., 2017) revealed a significant accumulation of peat under two vegetation types: swamp forests dominated by deciduous trees such as *Uapaca paludosa* Aubrév. & Leandri, *Carapa procera* DC. and *Xylopia rubescens* Oliv., and swamp forests dominated by palms, such as *Raphia laurentii* De Wild., or more rarely, *Raphia hookeri* G. Mann & H. Wendl., which occupy abandoned river channels (Dargie et al., 2017).

The vegetation of the plains is predominantly herbaceous, with the presence of floodplain forests within the interior regions. The best-drained areas are dominated by Poaceae, which includes species as *Jardinea congoensis* (Hack.) Franch., *Hyparrhenia diplandra* (Hack.) Stapf, *Digitaria leptorhachis* (Pilg.) Stapf, and *Panicum repens* L. Depressions and canal banks are characterised by the presence of Poaceae reeds (*Echinochloa pyramidalis* (Lam.) Hitchc. & Chase, *Echinochloa* sp., and other unidentified species), the Poaceae *V. cuspidata*, and Cyperaceae (*Cyperus papyrus* L.). The oil palm tree (*Elaeis guineensis* Jacq.) can be found in certain forest patches on the herbaceous plain (Comptour, 2017). The vegetation of the floodplain forest is characterised by that of the Lower Sangha rainforest region (White, 1983). These forests are mostly flooded during the rainy season, and occasionally during the dry season. The terrain is mainly swampy, consisting of flooded forests, periodically flooded forests, and *terra firme* forests. These forests have very shallow undergrowth, with palm thickets in places. The height of the trees varies between 15 and 30 m (Gilbert, 1984). The study area is characterised by the presence of forests dominated by *Lophira alata*, *G. demeusei*, *Mytragyna ledermannii*, and *Eremospatha cabrae*.

3. Material and methods

3.1. Sampling strategy

In May and June 2022, pooled leaf samples (approximately three to ten mixed shade and sun leaves) of common terrestrial and aquatic higher plant species and environmental water samples were collected in five different environments (savanna, village, open water, and

seasonally or perennially flooded swamp forest; see Fig. 1) in the central Congo Basin peatlands region (see **Supplementary Data 1 to 4**). Samples were collected at each site over of one or two days. The selection of sites was made on the basis of floristic diversity and the nature of the environment.

In the swamp forests, plant samples were collected at multiple sites (see Fig. 1b), including two transects situated near a fishing camp. These transects were conducted from the riverbank towards the peatlands. The transects ended where the vegetation became homogeneous. Transect 1 spanned a distance of 1,800 m, while transect 2 measured 600 m. In the rivers, the same dominant aquatic plant species was sampled, a helophyte known as 'hippopotamus grass' (*V. cuspidata*), which is rooted in mud and has both submerged and emergent parts, at different locations. A total of 53 leaf samples were collected from 25 sites for organic geochemical analysis. These samples represent 27 different plant species from 13 families. Each leaf sample was stored in a paper bag during the field sampling process, then in a paper press prior to being air-dried over the following days. Some plants were identified in the field using both local and scientific names. Samples of the unidentified plants were collected for subsequent identification at the National Herbarium (IRSEN) in Brazzaville. The scientific names of the species were verified using the African Plant Database website (https://www.africanplantdatabase.ch) of the Conservatoire et Jardin Botanique de la Ville de Genève, as referenced in Lebrun and Stork (2020). The identified species have been classified in their respective botanical families according to the APG IV classification for angiosperms (see **Supplementary Data 1**). Samples of environmental surface water were collected using a 0.2 μm pre-combusted glass fibre filter, and stored in 1.8 mL borosilicate glass vials with PTFE/silicone septa.

3.2. Analysis

3.2.1. Leaf biomass n-alkane identification and quantification

0.5 to 3 g of leaf powder was extracted using ultrasound for a time period of 20 min in 30 mL of a dichloromethane/methanol (9:1) solution. The total lipid extract (TLE) was separated from the solid leaf residue using 6 mL glass columns packed with 1.5 g of silica gel that had been dried at 60 °C. The TLEs were further purified by elution with hexane (10 mL) through a glass column containing $AgNO_3$- impregnated silica gel. The various homologues were analysed using a gas chromatograph equipped with a flame ionisation detector (GC-FID, ThermoScientific Trace GC) with a non-polar fused silica column (60 m x 0.25 mm x 0.1 μm, DB-5-MS (J&W)) and a deactivated retention gap (2.5 m x 0.53 μm). Hydrogen was utilised as the carrier gas, and the oven temperature was programmed in accordance with the following parameters: from 45 to 200 °C at a rate of 17 °C min^{-1}, from 200 to 250 °C at a rate of 5 °C min^{-1}, and from 250 to 300 °C at a rate of 3 °C min^{-1}. For the purpose of quantification, the FID peak areas of the *n*-alkanes were compared with those of an internal squalane standard and a *n*-C_{36} alkane standard. The abundances of *n*-alkanes in the leaves are expressed as μg g^{-1} dry leaf.

3.2.2. n-Alkane distribution indices

The distribution of long-chain *n*-alkanes can be characterised using various indices, including the ACL, the CPI and the carbon number maximum (C_{max}).

The ACL is a simple parameter for describing the distribution pattern of *n*-alkanes (Poynter et al., 1989). This represents the average chain length, weighted by the abundance of different carbon compounds. The ACL was calculated for *n*-alkanes ranging from *n*-C_{25} to *n*-C_{35} as follows:

$$ACL_{n-C25-n-C35} = \frac{\Sigma(n \times C_n)}{\Sigma(C_n)}$$

This parameter is commonly used to compare the composition of *n*-alkanes in plants as well as in palaeo-environmental and -climate studies to track vegetation and climate changes. Long-chain *n*-alkanes such as *n*-C_{33} and *n*-C_{35} have been identified as reliable indicators of C_4 grassland (monocots) ecosystems (Rommerskirchen et al., 2006; Vogts et al., 2009). In contrast, *n*-C_{27} and *n*-C_{29} have been shown to predominate in trees and shrubs (C_3 dicots; Cranwell, 1984; Meyers, 2003).

The odd–even ratio of carbon chain lengths is expressed by the CPI, calculated and slightly modified according to the methodology outlined by Bray and Evans (1961) as follows:

$$CPI = \frac{(n-C_{25}+n-C_{27}+n-C_{29}+n-C_{31}+n-C_{33}+n-C_{35})}{(n-C_{24}+n-C_{26}+n-C_{28}+n-C_{30}+n-C_{32}+n-C_{34})}$$

The distribution of *n*-alkanes in terrestrial plants generally shows a strong predominance of odd over even-numbered carbon homologues (Eglinton and Hamilton, 1967).

The C_{max} values are indicative of the predominant *n*-alkane homologue and can be used to differentiate between the dominant type of vegetation contributing to sedimentary *n*-alkanes (Liu et al., 2022). Consequently, the relative distribution of the dominant C_{max} was assessed across plant groups differing in photosynthetic pathway (C_3 vs. C_4) and growth form (monocots vs. dicots). The variation in the ratio of the two dominant *n*-alkane homologues *n*-C_{31}/(*n*-C_{29} + *n*-C_{31}) is also commonly used to estimate the contribution of C_3 and C_4 plant waxes to the sediments (Schefuß et al., 2003).

3.2.3. Leaf wax n-alkane $\delta^{13}C$ and δD analyses

$\delta^{13}C_{n\text{-alkane}}$ and $\delta D_{n\text{-alkane}}$ isotope analyses were performed at CEREGE using a ThermoScientific Trace GC coupled with a ThermoFisher Scientific Delta V^+ mass spectrometer via an Isolink II GC conversion unit. The GC itself was equipped with a TG5ms column (30 m × 0.25 mm × 0.25 μm), with helium serving as the carrier gas. The GC temperature was programmed to rise from 80 to 180 °C at a rate of 10 °C min^{-1}, and from 180 to 315 °C at a rate of 5 °C min^{-1} (for a duration of 16 min). For stable carbon isotope analysis, the combustion reactor was maintained at 1000 °C, and for hydrogen isotope analysis, the HTC pyrolysis reactor was held at 1420 °C. The samples were injected in duplicate in a random order.

The performance of the instrument and the H_3^+ factor were monitored daily using a reference H_2 gas and a mixture of *n*-alkanes with a known isotopic composition. During the period of analysis, the H_3^+ factor was found to be 3 ±0.08 (1 S.D.). The A7 *n*-alkane mixture (provided by Arndt Schimmelmann; Indiana University) was used as an external standard and run in duplicate every six injections to monitor the isotopic integrity over the analysis period. The standard deviation of all A7 mixture standards is better than 2‰ for δD and 0.4‰ for $\delta^{13}C$. The values of the $\delta D_{n\text{-alkane}}$ and the $\delta^{13}C_{n\text{-alkane}}$ are expressed in ‰ relative to the Vienna Standard Mean Ocean Water (V-SMOW) and the Vienna Pee Dee Belemnite (V-PDB), respectively.

The $\delta^{13}C_{n\text{-alkane}}$ values were determined using the same sample extract fraction as was used for the measurement of the $\delta D_{n\text{-alkane}}$ values. The $\delta^{13}C$ and δD values are presented for *n*-C_{27}, *n*-C_{29}, *n*-C_{31} and *n*-C_{33}, which are the most abundant *n*-alkanes (see **Supplementary Data 2 and 3**). The contemporary $\delta^{13}C$ values were corrected for variations in atmospheric $\delta^{13}C$ ($\delta^{13}C_{atm}$) associated with the Suess effect. This was achieved by adding the difference between the $\delta^{13}C_{atm}$ value at the time of sampling and the pre-industrial $\delta^{13}C_{atm}$ value (~2.2‰ lighter now than pre-industrial; Francey et al., 1999; McCarroll and Loader, 2004; Keeling et al., 2018) to the $\delta^{13}C$ value of each *n*-alkane (see **Supplementary Data 3**).

3.2.4. Environmental surface water δD and $\delta^{18}O$ values

To constrain the isotopic composition of plant water sources, we analysed the isotopic composition of river, pond water, and peat surface water collected near the study sites (see **Supplementary Data 4**). Analyses of environmental surface water δD and $\delta^{18}O$ (δD_{ESW} and $\delta^{18}O_{ESW}$, respectively) were conducted at MARUM using a Picarro 2130i Cavity

Ring-Down Spectrometer (CRDS) in high-precision mode. Nine injections of 1.8 μL each were performed using a 10 μL gastight syringe. The results are the average of the last three injections. Calibration was performed using VSMOW2, SLAP2, and a laboratory-internal standard, as well as mixtures thereof with SLAP2. The isotopic composition of precipitation from GNIP stations (IAEA/WMO, 2020) bordering the CCB (i.e., Bangui, Kinshasa, and Kisangani) were further used as reference values for comparison with our local δD_{ESW} and $\delta^{18}O_{ESW}$ data (see Section 4.6).

3.2.5. Leaf wax hydrogen isotopes fractionation

In order to evaluate the influence of vegetation and other environmental factors on the $\delta D_{n\text{-alkane}}$ values in the CCB, we calculated the difference between the $\delta D_{n\text{-alkane}}$ values and the δD_{ESW} values ($\varepsilon_{n\text{-alkane/ESW}}$) as follows:

$$\varepsilon_{n-\text{alkane/ESW}} = \left(\frac{\delta D_{n-\text{alkane}} + 1000}{\delta D_{ESW} + 1000} - 1\right) \times 1000$$

This difference is often referred to as 'apparent fractionation' (ε_{app}), since it encompasses D-enrichment during the evaporation of soil and leaf water and during wax biosynthesis (Smith and Freeman, 2006; Sachse et al., 2012).

3.2.6. Statistical tests

To facilitate comparisons between plant groups, statistical analyses were performed between angiosperm subclasses (monocots vs. dicots) and photosynthetic pathways (C_3 vs. C_4). Student's t-tests were applied when data met the assumptions of normality and homogeneity of variance. When these conditions were not satisfied or were uncertain, particularly for small sample sizes, non-parametric Wilcoxon rank-sum tests were used (see **Supplementary Data 5 and 6**). All analyses were carried out using the rstatix package (Kassambara, 2023) in the R language (R Core Team, 2022).

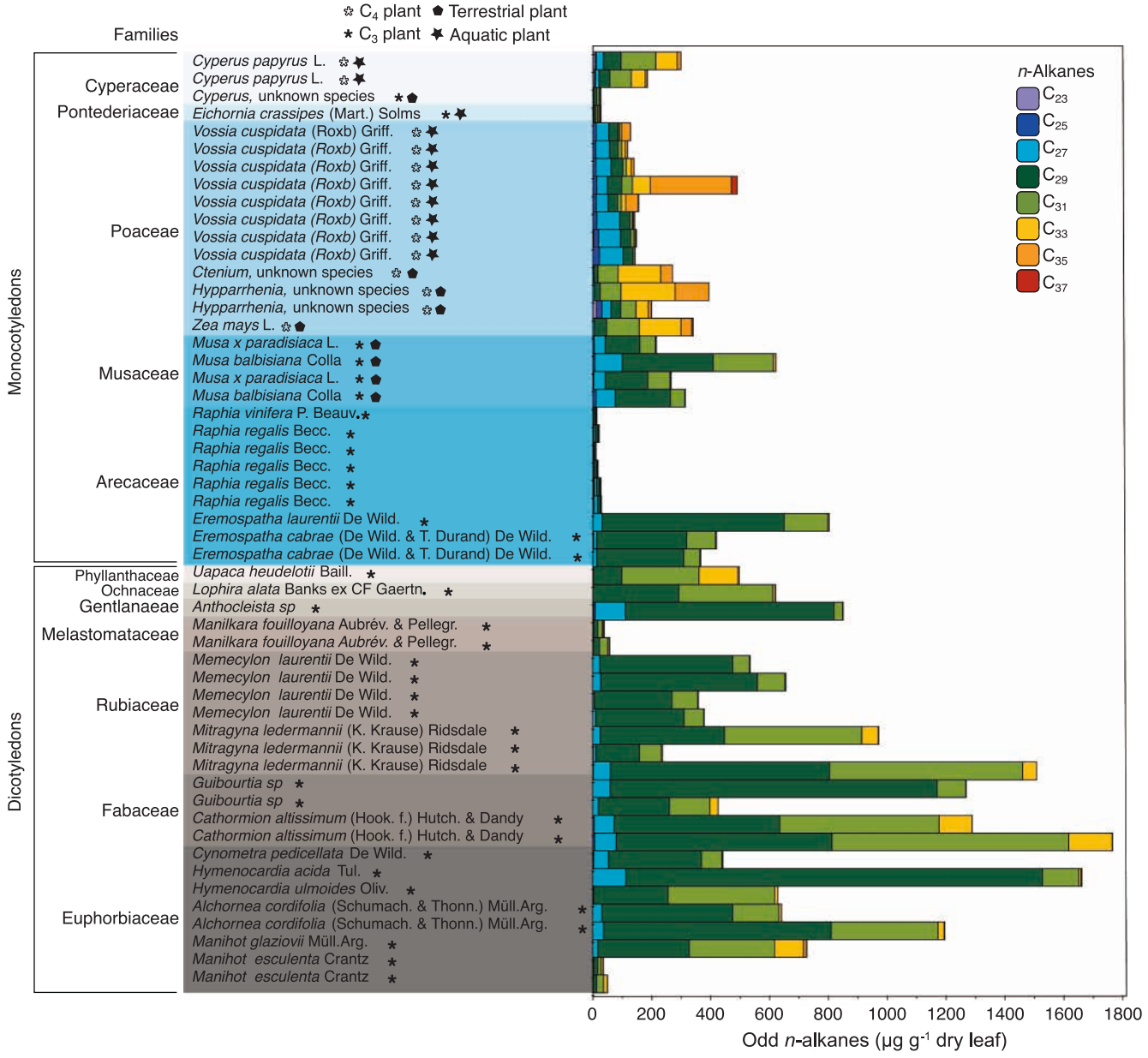

Fig. 3. Odd-chain *n*-alkanes homologues abundances (μg g^{-1} dry leaf) from sampled living plants in the CCB. (For interpretation of the references to colour in this figure legend, the reader is referred to the web version of this article.)

4. Results and discussion

4.1. n-Alkane abundances

The abundances of *n*-alkanes from living plants in the CCB are presented in Fig. 3. We detect *n*-alkanes from *n*-C_{23} to *n*-C_{37} in our dataset, with a notable predominance of *n*-C_{29} and *n*-C_{31} (Fig. 3), which may be reflected in peat deposits as the two predominant homologues contributing to the sedimentary *n*-alkanes. In general, C_3 (with the exception of *Raphia* sp.) and/or dicots have been found to synthesise more *n*-alkanes than C_4 and/or monocots. This has the potential to obscure the *n*-alkane extracted from palaeo-environmental archives by introducing a total *n*-alkane skewed towards C_3 dicots plants (Fig. 3). The longest *n*-alkane homologues (*n*-C_{33} to *n*-C_{37}) are found in greater abundance in C_4 plants, although significant levels are also synthesised in some C_3 plants (Fig. 3).

4.2. Stable carbon isotope composition of n-C_{29} alkanes

At the ecosystem level, as per previous studies (e.g., Castañeda et al., 2009; Vogts et al., 2009; Schefuß et al., 2011; Yang and Bowen, 2022), *n*-C_{29} alkane is generally the most abundant *n*-alkane extracted from sedimentary archives. It is frequently used for palaeo-climatic reconstructions, occasionally in combination with the *n*-C_{31} homologue. This dominance can be attributed, at least in part, to the type of source vegetation: it is evident from Fig. 3 that C_3 plants produce a greater amount of *n*-alkane, with *n*-C_{29} and *n*-C_{31} being the most abundant chain lengths. The C_3 plants have $\delta^{13}C_{n\text{-}C29}$ values ranging from −40.7 to −30‰, i.e., significantly lower than those of C_4 plants (ranging from −21.4 to −17.2‰; see Fig. 4). The $\delta^{13}C_{n\text{-alkane}}$ values in C_4 plants are on average, ~17‰ higher and significantly less variable than those measured in C_3 plants. Despite the fact that C_3 plants synthesise up to one order of magnitude more waxes than C_4 plants, C_4 plants still synthesise significant amounts of *n*-C_{29} (Fig. 4a) and cover ACL (Fig. 4d) and CPI (Fig. 4g) ranges at least as large as for C_3 plants. The $\delta^{13}C_{n\text{-}C29}$ and/or $\delta^{13}C_{n\text{-}C31}$ remain the most effective tracers for the predominant photosynthetic pathway in sedimentary archives. From our dataset, it is difficult to discriminate between plant families on the basis of $\delta^{13}C_{n\text{-}C29}$, ACL or CPI values (Figs. 4b, e, h). We note that among the four analysed species of palm trees, CPI and ACL do not draw a clear picture at the species level (Figs. 4f, i), and that *Raphia* sp., which has overall low *n*-alkane abundances, may not contribute significantly to sedimentary *n*-alkanes (Figs. 3 and 4c).

4.3. n-Alkane distribution indices

Within our dataset, the *n*-alkane distribution indices that are commonly used in palaeo-climate and palaeo-environmental studies (ACL, CPI, C_{max}, and *n*-C_{31}/(*n*-C_{29} + *n*-C_{31})) do not permit the distinction between photosynthetic pathways or angiosperm subclasses (see Figs. 5a–d, f–i, k–n, p–s, 'Congo' dataset and **Supplementary Data 1 and 5**). A similar pattern is observed when the comparison is extended to include data from the African continent as a whole (Figs. 5a–d, f–i, k–n, p–s, 'All Africa' dataset and **Supplementary Data 5 and 7**). Yet, a striking observation in the odd *n*-alkanes distribution in our Congo dataset (Fig. 3) indicates that the *n*-C_{29} homologue, which is frequently the most abundant sedimentary *n*-alkane and subsequently used for isotopic analysis, is occasionally less dominant than the shorter *n*-C_{27} in specific Poaceae (e.g., *V. cuspidata*) and frequently less dominant than the longer *n*-C_{33} and *n*-C_{35} in Poaceae and Cyperaceae. We hence computed a new index referred to as GRIND (GRaminoid INDex) to take into account this distinction in the dicot vs. monocot *n*-alkane homologue distribution as follows: (*n*-C_{27} + *n*-C_{33} + *n*-C_{35})/(*n*-C_{25} + *n*-C_{27} + *n*-C_{29} + *n*-C_{31} + *n*-C_{33} + *n*-C_{35}) (Figs. 5e, j, o, t, 'Congo' dataset). GRIND ranges between ~0.2 ($n = 39$) in C_3 plants and ~0.6 ($n = 14$) in C_4 plants (Figs. 5e, j) and between ~0.1 ($n = 24$) in dicots and ~0.5 ($n = 29$) in monocots (Figs. 5o, t). When the index is applied to the available African data, it emerges that a clear distinction can be established between C_3 and C_4 plants as well as between dicots and monocots (Figs. 5e, j, o, t, 'All Africa' dataset). This distinction is significantly more pronounced than that observed with other indices presented in Fig. 5. For both datasets, GRIND is significantly different for C_3 plants against C_4 plants and for dicots against monocots (p-value (p) < 0.001; see **Supplementary Data 5**). We propose this ratio as a new tool in palaeo-environmental reconstructions.

Ratios such as (*n*-C_{27} + *n*-C_{29})/(*n*-C_{27} + *n*-C_{29} + *n*-C_{31}) have traditionally been used to estimate the contribution of woody dicotyledons to sedimentary *n*-alkanes (Zhang et al., 2008). However, these early approaches frequently overlook the long-chain homologues that are characteristic of grasses. In order to address this issue, the GRIND index incorporates *n*-C_{27}, *n*-C_{33}, and *n*-C_{35} — compounds that are typically more abundant in grasses, particularly C_4-dominated species, and in sedges. Studies show that long-chain *n*-alkanes (*n*-C_{33} and *n*-C_{35}) occur in much higher proportions in grasses than in most woody plants (Rommerskirchen et al., 2006; Tweedy et al., 2025). This finding is consistent with the broader trends observed in *n*-alkane distributions, where woody plants (i.e., trees and shrubs) exhibit maxima at *n*-C_{27} or *n*-C_{29}, while grasses and herbs reach their peak at *n*-C_{31} or *n*-C_{33} (Cranwell, 1984; Meyers, 2003; Krull et al., 2006; Vogts et al., 2009; Garcin et al., 2014; Liu et al., 2018, 2022). Alternative ratios, such as *n*-C_{29}/*n*-C_{31}, *n*-C_{31}/(*n*-C_{29} + *n*-C_{31}), *n*-C_{31}/(*n*-C_{27} + *n*-C_{31}), *n*-C_{33}/(*n*-C_{29} + *n*-C_{33}), *n*-C_{35}/(*n*-C_{29} + *n*-C_{35}), and *n*-C_{33}/(*n*-C_{25} + *n*-C_{27} + *n*-C_{29} + *n*-C_{31} + *n*-C_{33} + *n*-C_{35}), have been proposed to differentiate between woody and herbaceous vegetation in savanna environments (Schefuß et al., 2003; Vogts et al., 2009; Bush and McInerney, 2013).

If the GRIND index seems a useful complementary tool for estimating the vegetation cover, it may be affected by uncertainties related for example to production of *n*-C_{33} alkanes by some C_3 species or by the low concentrations of long-chain *n*-alkanes in some sedimentary deposits. Further testing across tropical regions and integration with other proxies (e.g., pollen and $\delta^{13}C$) will help validate this index for reconstructing past C_3/C_4 vegetation dynamics.

4.4. Stable carbon isotope composition combined with abundances in n-C_{27}, n-C_{29}, n-C_{31}, and n-C_{33} alkanes

The vegetation cover at the ecosystem level integrates plants over a mosaic of plant functional types (PFTs). When incorporated into sediments and/or peat deposits, the lipid extracts containing the *n*-alkanes used for $\delta^{13}C$ measurements predominantly reflect input from the most abundant plants. However, they can be skewed towards plants that produce very high concentrations of *n*-alkanes, which may dominate the sedimentary isotopic signal, such as, e.g., C_3 dicots for *n*-C_{29} (see Figs. 3 and 6 and **Supplementary Data 3**).

Given the large spectrum of environments sampled during the field campaign (Figs. 1 and 2) and the potential for varying PFTs to obscure the sedimentary *n*-alkane signal in palaeo-environmental reconstructions, the $\delta^{13}C_{n\text{-alkane}}$ of each leaf sample collected during the field campaign were reported according to their PFT and their relative abundance for the four dominant odd *n*-alkanes (i.e., from *n*-C_{27} to *n*-C_{33}, Fig. 6). It should be noted that the choice to represent the $\delta^{13}C$ as a function of latitude is only for visual convenience. Across the latitudinal transect, the southernmost sampling sites were dominated by samples composed of leaves of C_4 monocots (PFT 'aquatic herbs', see Fig. 6, as illustrated in Figs. 2c, d), transitioning towards samples of palms (Fig. 2b), trees (Fig. 2a), as well as terrestrial herbs and shrubs such as those found in grass-dominated savannas (Figs. 2e and 6). It can be hypothesised that a sediment or peat sample collected at the confluence of these environments would likely demonstrate a *n*-C_{27} to *n*-C_{33} distribution, with a strong predominance of inputs from C_3 plants. This would be particularly evident when considering the $\delta^{13}C$ values of *n*-C_{29} and *n*-C_{31} (Fig. 6), i.e., the homologues most commonly used in palaeo-

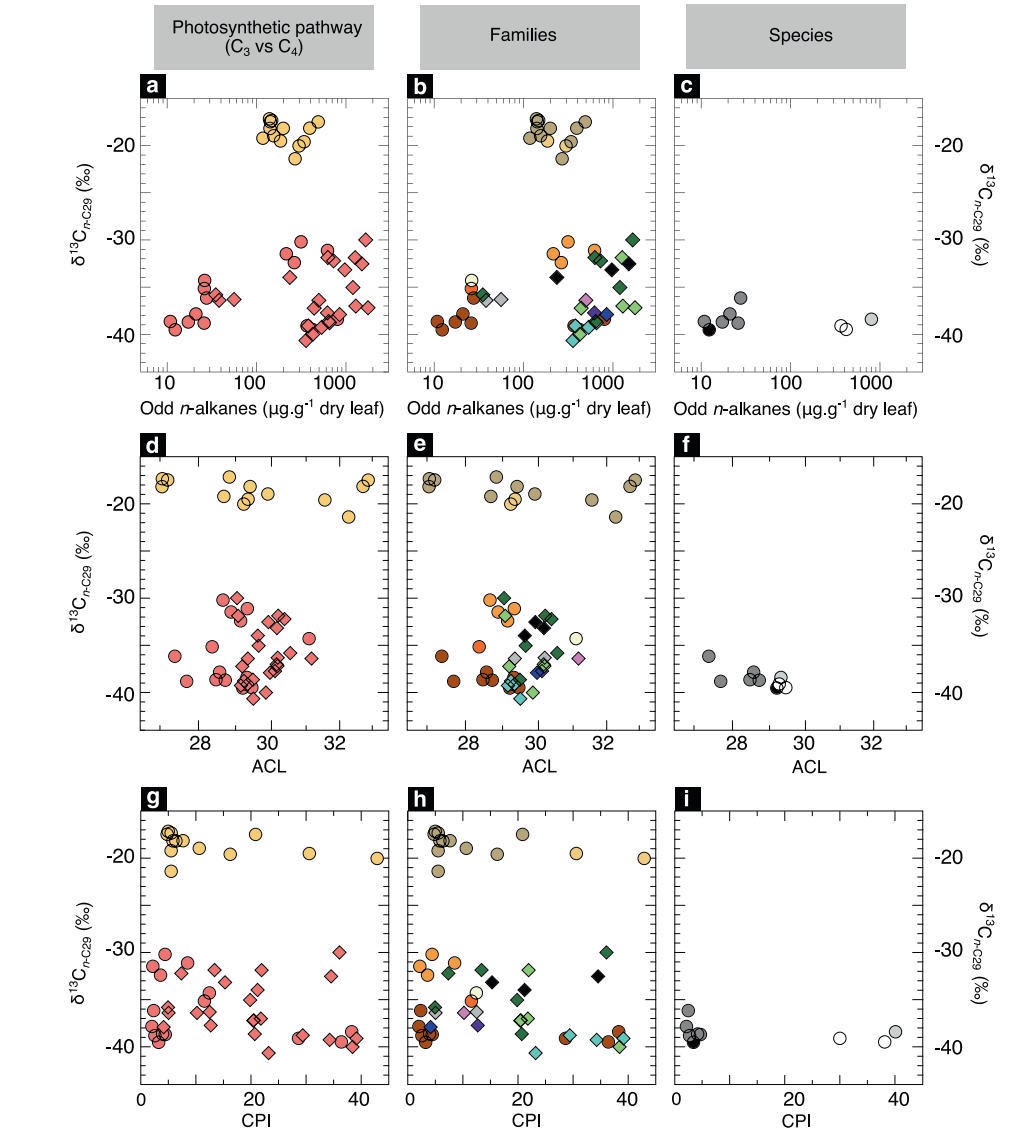

Fig. 4. Comparison of $\delta^{13}C_{n\text{-}C29}$ values with odd *n*-alkanes abundances, ACL, and CPI, according to photosynthetic pathways (a, d, g), monocots (black circle outline) vs. dicots (black diamond outline) angiosperm subclasses (a, b, d, e, g, h), families (b, e, h), and species of the Arecaceae family (c, f, i). (For interpretation of the references to colour in this figure legend, the reader is referred to the web version of this article.)

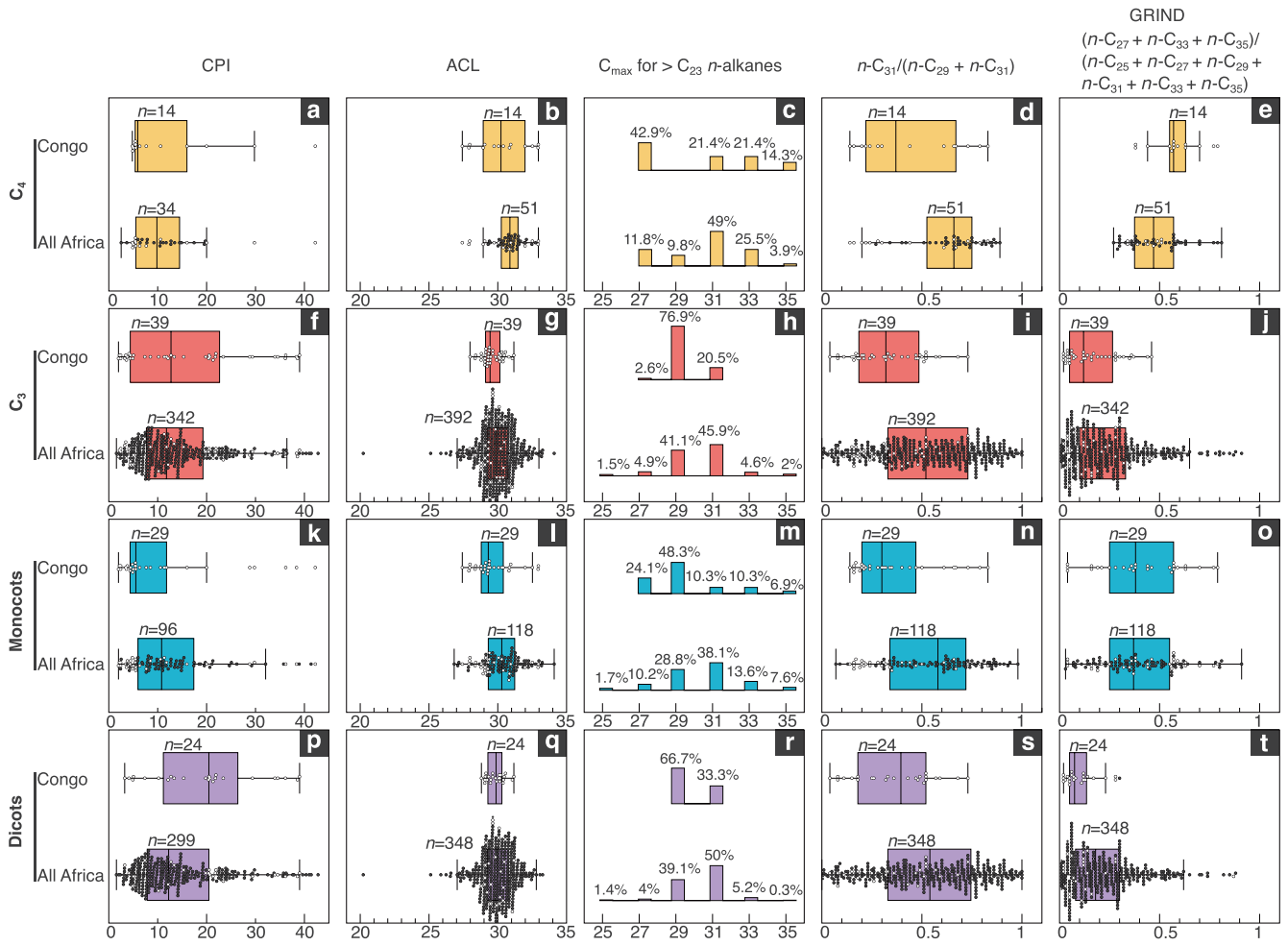

Fig. 5. Compilation of *n*-alkane distribution indices from living plants for C_3 plants (a—e) and C_4 plants (f—j), and monocots (k—o) and dicots (p—t). Two datasets are compared: 'Congo' data (this study; white dots) and 'All-Africa' data (this study (white dots) and all other available data (black dots); see Supplementary Data 7). CPI (a, f, k, p), ACL (b, g, i, q), C_{max} (c, h, m, r), the ratio (*n*-C_{31})/(*n*-C_{29} + *n*-C_{31}) (d, i, n, s), and the GRIND index (e, j, o, t). (For interpretation of the references to colour in this figure legend, the reader is referred to the web version of this article.)

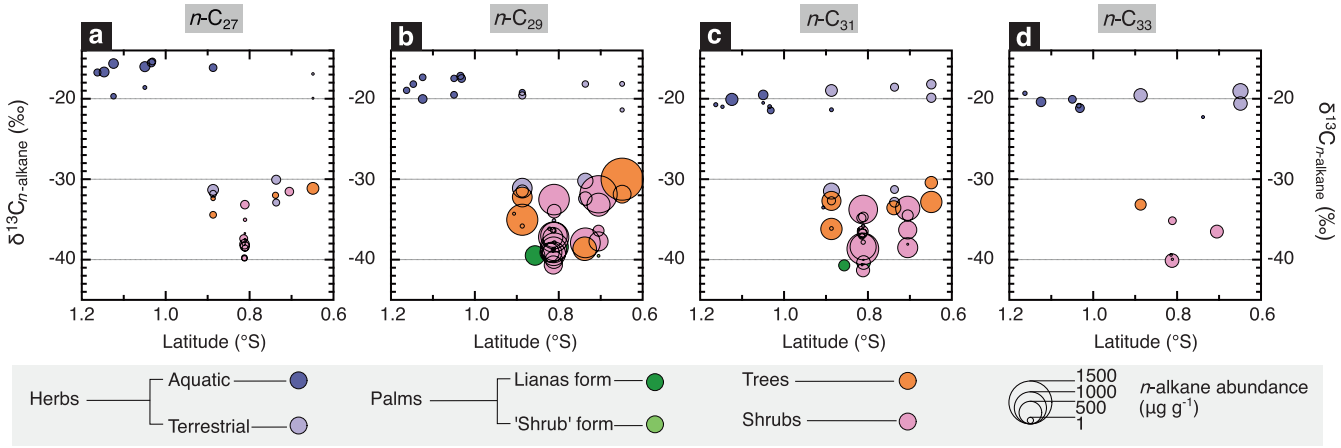

Fig. 6. $\delta^{13}C_{n\text{-alkane}}$ values and *n*-alkane abundances from living plants in the CCB shown against latitude. (a) *n*-C_{27} alkane, (b) *n*-C_{29} alkane, (c) *n*-C_{31} alkane, and (d) *n*-C_{33} alkane. (For interpretation of the references to colour in this figure legend, the reader is referred to the web version of this article.)

environmental reconstructions. However, it is important to note that this apparent C_3 signal may still include a secondary, though non-negligible, contribution from *n*-alkanes synthesised by C_4 graminoids (Fig. 6). This finding emphasises the importance of integrating the isotopic composition of *n*-alkane and the associated sedimentary pollen assemblages in tandem when attempting to accurately interpret the $\delta^{13}C$ values of sedimentary *n*-alkanes (e.g., Feakins, 2013; Garcin et al., 2022).

4.5. Hydroclimate conditions influence on the $\delta^{13}C_{n\text{-alkane}}$ of African leaves

As already observed in various parts of Africa, the data presented here demonstrate that the photosynthetic pathway is the main driver of $\delta^{13}C_{n\text{-alkane}}$, and that there is a high degree of variability in the $\delta^{13}C$ values of C_3 plants sampled in different environments (e.g., Rommerskirchen et al., 2006; Vogts et al., 2009; Garcin et al., 2014; Badewien et al., 2015; Gensel et al., 2022). Other factors potentially influencing the $\delta^{13}C$ values in C_3 leaves may be related to water limitation and/or canopy closure. Water limitation is known to drive ^{13}C enrichment in leaves, as stomata regulate water loss and hence drive carbon dioxide limitation (Farquhar et al., 1989). However, while this factor may be relevant in dry environments, it is not expected to be significant in the CCB peatlands region, where relative humidity (RH) remains high throughout the year (80–90%; Samba et al., 2023). The variability in $\delta^{13}C_{n\text{-alkane}}$ values may also be influenced by the distinction between canopy (sunlit leaves) and understorey (shaded leaves), with sunlit leaves being ^{13}C-enriched relative to shaded leaves (Farquhar et al., 1989; Graham et al., 2014; Wu et al., 2017). Another key factor which may impact understorey vegetation is the 'canopy effect' (Van Der Merwe and Medina, 1991), involving the recycling of ^{13}C-depleted CO_2 derived from microbial soil respiration in the understorey of closed-canopy forests, as well as fractionation due to photosynthesis under low light conditions. This results in ^{13}C depletion of C_3 leaves (Graham et al., 2014). Our results agree with other field studies on leaf waxes, which show occasionally highly negative $\delta^{13}C_{n\text{-alkane}}$ values, and which are similarly interpreted as resulting from a combination of water availability (high mean annual precipitation and/or high annual RH) and canopy effect under closed-canopy conditions and low light intensity (Garcin et al., 2014; Wu et al., 2017).

In tropical peatland ecosystems such as those of the central Congo Basin, methane is typically highly ^{13}C-depleted, and its microbial oxidation produces isotopically light CO_2 (Holmes et al., 2015). This CH_4-derived CO_2 could, in principle, contribute to the formation of highly negative $\delta^{13}C$ values in plant biomass and associated *n*-alkanes. Clear demonstrations of CH_4-derived carbon assimilation exist for *Sphagnum* mosses, which form close symbioses with methanotrophic bacteria (Raghoebarsing et al., 2005; Van Winden et al., 2020). However, firm evidence that vascular plants assimilate this CO_2 in sufficient quantities to alter their bulk $\delta^{13}C$ remains lacking, but given the small relative contribution of CH_4 oxidation to the total CO_2 available for photosynthesis, any influence on vascular plant $\delta^{13}C$ would likely be minimal. Consequently, while the CH_4 oxidation may exert a localized and subtle isotopic effect, the very wet conditions and the canopy effect remain the most robust and consistent explanation for the very low $\delta^{13}C$ values observed in the biomass of vascular plants in tropical peatlands.

As illustrated in Fig. 7, the $\delta^{13}C_{n\text{-alkane}}$ values (see **Supplementary Data 8**) of living plants in Congo were compiled alongside those from other African sites (i.e., Rommerskirchen et al., 2006; Vogts et al., 2009; Kristen et al., 2010; Bezabih et al., 2011; Garcin et al., 2014; Badewien et al., 2015). These data are compared with mean annual RH (Hersbach et al., 2020) to determine if variations in $\delta^{13}C_{n\text{-alkane}}$ values are related to continental-scale climate conditions (Winter, 1981; Farquhar et al., 1982; Madhavan et al., 1991). The combined plant data for Africa cover a RH range of 40–90%, with discontinuous data below 40% RH. The $\delta^{13}C_{n\text{-alkane}}$ values of African C_4 plants mostly do not show significant variability following different RH classes (see **Supplementary Data 6** and Fig. 7). Conversely, the $\delta^{13}C_{n\text{-alkane}}$ values of African C_3 plants do not differ significantly between 40 and 80% RH, but differ significantly (Wilcoxon test ($p < 0.05$)), with lower mean value of −37‰ above 80% RH (Fig. 7).

These results suggest that $\delta^{13}C_{n\text{-alkane}}$ may be used to track very wet environments, in African and other tropical regions. Dense forest cover, where factors such as the 'canopy effect' (Van Der Merwe and Medina, 1991) could lead to substantial ^{13}C-depletion in the leaves of understorey vegetation, are often associated with high RH. Extending our findings to sedimentary leaf waxes, which are commonly used as palaeoenvironmental proxies in Africa (Rommerskirchen et al., 2003; Schefuß et al., 2003; Niedermeyer et al., 2010; Feakins, 2013; Garcin et al., 2014) suggests that very negative $\delta^{13}C$ values of sedimentary leaf waxes (i.e., < –37‰), predominantly derived from C_3 plants, may reflect high RH conditions (> 80%) in the past and may therefore help with palaeoclimatic reconstructions.

4.6. Stable hydrogen isotope composition in environmental waters and its $\delta D_{n\text{-}C29}$ and $\delta D_{n\text{-}C31}$ counterparts

The precipitation isotopic composition of the GNIP stations (IAEA/WMO, 2020) bordering the CCB indicates precipitation δD (δD_{precip}) that vary in a range comprised between ~–35 and ~+30‰ during the dry and rainy seasons, respectively, with seasonal and mean annual values varying with sites (Fig. 1a). When these values are weighted against the monthly mean amount of precipitation, the annual δD_{precip} values are

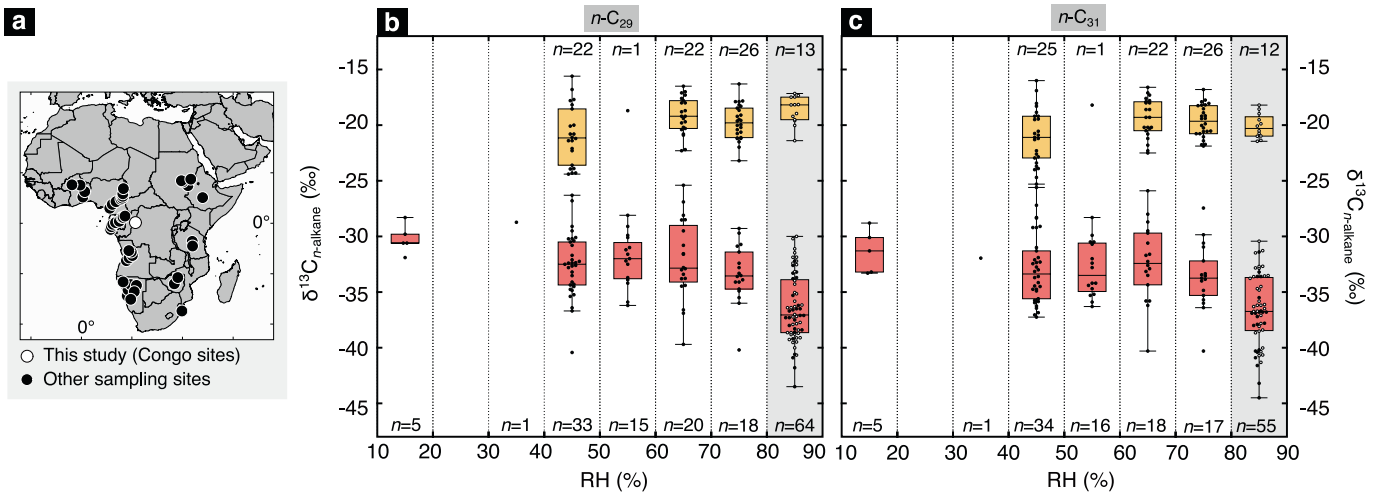

Fig. 7. (a) Map of African study sites where $\delta^{13}C_{n\text{-C29}}$ and $\delta^{13}C_{n\text{-C31}}$ values in plant samples are available (white dots: this study, black dots: other studies; see Supplementary Data 8). (b) $\delta^{13}C_{n\text{-C29}}$ values against relative humidity (Hersbach et al., 2020). (c) $\delta^{13}C_{n\text{-C31}}$ values against relative humidity. (b and c) Data are binned using 10%-RH bins; C_4 and C_3 plant data are shown in yellow and in red, respectively (white dots: this study, black dots: other studies); vertical grey bands indicate RH > 80%. (For interpretation of the references to colour in this figure legend, the reader is referred to the web version of this article.)

skewed towards negative values (Fig. 1a). In a $\delta D/\delta^{18}O$ scatterplot (Fig. 8a), The GNIP data is reported alongside the environmental surface water samples collected *in situ*. The stable isotope values of the sampled environmental surface waters overlap with the available precipitation data from the three local GNIP stations (Kinshasa, Bangui, and Kisangani). This suggests that δD_{ESW} and $\delta^{18}O_{ESW}$ probably track the isotopic composition of precipitation with minimal influence from evaporation processes. We cannot rule out the possibility that under more arid conditions, environmental surface waters were more influenced by evaporation and plant transpiration was significantly enhanced. However, at a global scale, the $\delta D_{n\text{-alkane}}$ values are largely controlled by δD_{precip} values; only in hyperarid zones they are additionally influenced by evapotranspirative D-enrichment (Gaviria-Lugo et al., 2023). Since arid conditions are necessarily associated with higher δD_{ESW} values, we argue that evapotranspiration increase would help identify subtle changes in hydroclimate.

Both temperature and hydroclimate affect the δD of the environmental water ultimately used by terrestrial and aquatic photosynthesising organisms. However, the process of lipid biosynthesis and other second-order parameters affecting the intracellular plant (leaf) water strongly fractionate the hydrogen isotope composition in the resulting $\delta D_{n\text{-alkane}}$ values (Sachse et al., 2012). This isotopic fractionation during lipid biosynthesis results in the systematic lowering of the $\delta D_{n\text{-alkane}}$ by ~–200 to ~−100‰ in our dataset (Fig. 8b). The broad range in the $\delta D_{n\text{-C29}}$ values presented in Fig. 8b is attributable to the fact that the entire dataset contains plants with contrasting photosynthetic pathways, monocots and dicots, contrasting PFTs, and which were sampled in contrasting environments. In Fig. 9 we detail these contrasting $\delta D_{n\text{-alkane}}$ values associated with different plant samples.

The $\delta D_{n\text{-alkane}}$ values of C_3 plants ($\delta D_{n\text{-C29}}$ = –150 ±21‰ (n = 36) and $\delta D_{n\text{-C31}}$ = –145 ±23‰ (n = 29)) are D-enriched compared to those of C_4 plants ($\delta D_{n\text{-C29}}$ = –182 ±22‰ (n = 14) and $\delta D_{n\text{-C31}}$ = –176 ±18‰ (n = 14); Figs. 9a, b). This pattern is reflected in the $\varepsilon_{n\text{-alkane/ESW}}$ values of C_3 plants (monocots and dicots; $\varepsilon_{n\text{-C29/ESW}}$ = −141 ±20‰ (n = 36) and $\varepsilon_{n\text{-C31/ESW}}$ = −136 ±22‰ (n = 14)) as compared to those of C_4 plants (monocots; $\varepsilon_{n\text{-C29/ESW}}$ = −172 ±24‰ (n = 14) and $\varepsilon_{n\text{-C31/ESW}}$ = −166 ±17‰ (n = 14); Figs. 9c, d).

Analogously to the photosynthetic pathway, the monocots vs. dicots have drastically different $\delta D_{n\text{-alkane}}$ values, with dicots being D-enriched compared to monocots. The $\delta D_{n\text{-C29}}$ and $\delta D_{n\text{-C31}}$ for dicots have values of −142 ±19‰ (n = 22) and −139 ±21‰ (n = 21), respectively, while the $\delta D_{n\text{-C29}}$ and $\delta D_{n\text{-C31}}$ for monocots have values of −173 ±22‰ (n = 27) and −171 ±21‰ (n = 22), respectively (Fig. 9).

Within monocots, aquatic herbs in C_4 ($\delta D_{n\text{-C29}}$ =–180 ±24‰, n = 10; $\delta D_{n\text{-C31}}$ = –168 ±16‰, n = 11) and terrestrial herbs in C_4 and C_3 ($\delta D_{n\text{-C29}}$ = –180 ±22‰, n = 8; $\delta D_{n\text{-C31}}$ = –177 ±27‰, n = 9) are more D-depleted than palms with a liana growth form ($\delta D_{n\text{-C29}}$ = –155 ±7‰, n = 3; $\delta D_{n\text{-C31}}$ = –157‰, n = 1) or with shrub form ($\delta D_{n\text{-C29}}$ = –154 ±5‰, n = 5; $\delta D_{n\text{-C31}}$ = –149‰, n = 1; **Supplementary Data 9**). Within dicots, shrubs are more D-depleted than hardwood trees, with $\delta D_{n\text{-C29}}$ and $\delta D_{n\text{-C31}}$ mean values for shrubs of −155 ±27‰ and −153 ±23‰, respectively, and $\delta D_{n\text{-C29}}$ and $\delta D_{n\text{-C31}}$ mean values for hardwood trees of −138 ±13‰ and −133 ±12‰, respectively, i.e., representing the less D-depleted n-alkanes among the studied PFTs (**Supplementary Data 9**). Again, these isotopic patterns translate into $\varepsilon_{n\text{-alkane/ESW}}$ fingerprint among PFTs (**Supplementary Data 9**).

The $\delta D_{n\text{-alkane}}$ values of flooded savanna plants are the most D-depleted, with $\delta D_{n\text{-C29}}$ = –193 ±8‰ (n = 8) and $\delta D_{n\text{-C31}}$ = –176 ±5‰ (n = 8). The $\delta D_{n\text{-alkane}}$ of savanna plants are less D-depleted, with $\delta D_{n\text{-C29}}$ = –164 ±21‰ (n = 4) and $\delta D_{n\text{-C31}}$ = −167 ±33‰ (n = 4). Swamp forest plants, that mainly consist in C_3 dicots, overlap their isotopic composition with the C_3 and dicot subgroups (Fig. 9).

Note that, in addition to our δD_{ESW} values being only an approximation of the δD_{precip} values commonly used in the literature to calculate ε_{app}, our isotopic dataset for potential plant water is likely incomplete. This is due to the fact that the sampled waters do not necessarily reflect the actual source water used by plants during biosynthesis, depending on whether n-alkane synthesis occurs primarily during the rainy season or over a longer period throughout the year. On a global scale, the ε_{app} between plant wax n-alkanes and source water (prevalently precipitation) spans a wide range of approximately ~−200 to ~−20‰, reflecting both biochemical and environmental controls (Sachse et al., 2012; Liu et al., 2023). A relatively constant biosynthetic fractionation of ~−150‰ occurs during the conversion of leaf water to n-alkanes, while variability in ε_{app} mostly arises from differences in leaf-water D-enrichment and plant ecophysiology (Sachse et al., 2012; Kahmen et al., 2013). Systematic offsets are observed among PFTs (Sachse et al., 2012): C_3 grasses typically exhibit more negative apparent fractionation values (−157 ±29‰), C_4 grasses less negative values (−141 ±21‰), and woody C_3 plants the least negative (−117 ±29‰). These differences are attributed to a combination of photosynthetic pathway effects, growth form (woody vs. grassy), and environmental conditions such as humidity, aridity, and canopy structure, all of which influence the extent of leaf-water evaporative D-enrichment (Tipple and

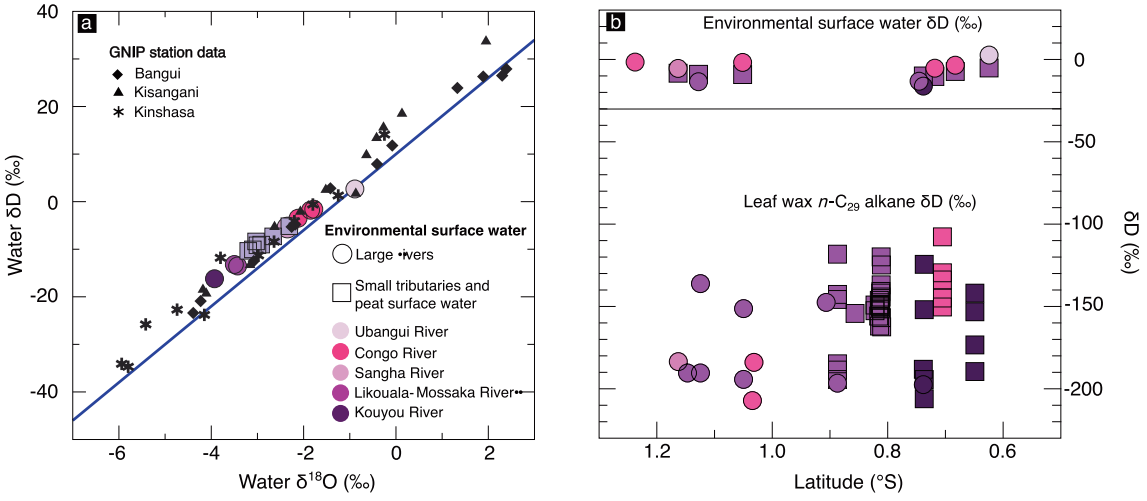

Fig. 8. (a) Hydrogen and oxygen isotope ratios of environmental surface waters in the CCB peatlands compared with GNIP precipitation data (monthly means) from Kinshasa, Bangui, and Kisangani (IAEA/WMO, 2020). Also shown in blue line is the global meteoric water line (GMWL). (b) Variability of δD_{ESW} (top) and $\delta D_{n\text{-C29}}$ for living plants (bottom) in the CCB peatlands region shown against latitude. (For interpretation of the references to colour in this figure legend, the reader is referred to the web version of this article.)

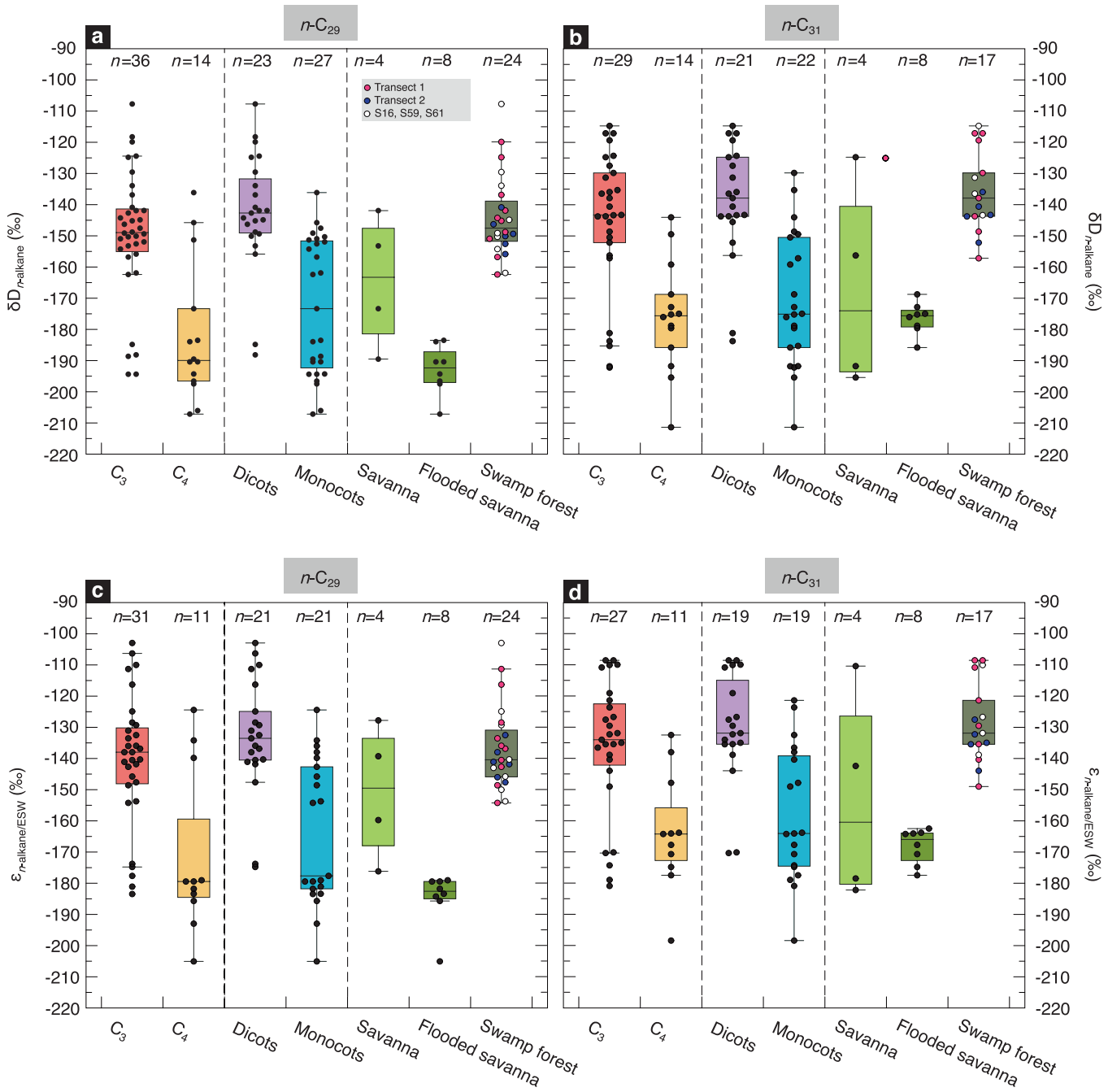

Fig. 9. $\delta D_{n\text{-alkane}}$ and $\varepsilon_{n\text{-alkane/ESW}}$ values for living plants in the CCB peatlands region: (a) $\delta D_{n\text{-C29}}$, (b) $\delta D_{n\text{-C31}}$, (c) $\varepsilon_{n\text{-C29/ESW}}$, (d) $\varepsilon_{n\text{-C31/ESW}}$. Coloured boxes indicate photosynthetic pathways (C_3 vs. C_4), angiosperm subclasses (dicots vs. monocots), and local environments (savanna, flooded savanna, and swamp forest). (For interpretation of the references to colour in this figure legend, the reader is referred to the web version of this article.)

Pagani, 2013). The plant dataset from the central Congo Basin clearly demonstrates the well-known systematic different ε_{app} values between woody C_3 plants and C_4 grasses (see $\varepsilon_{n\text{-alkane/ESW}}$, Figs. 9c, d). We also note that our limited data show more negative ε_{app} values (C_4 plants: −172 ±24‰ and C_3 plants: −141 ±20‰, see above) compared to other existing ε_{app} compilations (Sachse et al., 2012; Liu et al., 2023). These disparities may be attributed to the definition of the source water used in the calculation of ε_{app} (annual vs. seasonal precipitation, soil water, groundwater, small water stream, or river water) and the timing of wax production, given that wet-season biosynthesis from isotopically lighter precipitation can drive apparent fractionation to more negative values (Liu et al., 2023). However, on global scale, the most negative ε_{app} values are predominantly found in the wettest environments (Sachse et al., 2012; Gaviria-Lugo et al., 2023) — as those found in the study area.

As shown in Fig. 3, accounting for variations in *n*-alkane production among plants and the prevalence of C_3 biomass at the sampled locations (see Fig. 2) suggests that the resulting sedimentary *n*-alkane characteristics are predominantly skewed towards C_3 dicot plants, both in the *n*-alkane homologue distribution (see Section 4.4) and their associated δD, despite the presence of graminoids in wet equatorial environments. Drastic hydroclimate changes could induce widespread shifts in dominant vegetation at tropical latitudes. Such shifts have been observed in Africa during glacial-interglacial timescales (e.g., Tierney et al., 2010) and at the onset and termination of the last African Humid Period (e.g., Shanahan et al., 2015; Jaeschke et al., 2020). In such cases, the use of

$\delta^{13}C_{n\text{-alkane}}$ records has been demonstrated as a means to estimate vegetation composition (C_3 vs. C_4) and to correct for the effects of vegetation on $\delta D_{n\text{-alkane}}$ records (Collins et al., 2013; Wang et al., 2013; Shanahan et al., 2015; Tierney et al., 2017; Garcin et al., 2018). This approach, when combined with pollen data (e.g., Feakins, 2013), allows the hydroclimate signal to be isolated from vegetation influences.

5. Conclusion

We conducted a survey of the distribution and the stable carbon and hydrogen isotope composition of leaf wax *n*-alkanes in savannas, rivers, and forests within the peatlands of the central Congo Basin area. The present study demonstrates the potential of leaf wax biomarkers for various applications, including palaeo-environmental and -climatic reconstructions in Central Africa and beyond.

Based on the distribution of the different *n*-alkane homologues in the analysed plant samples, we proposed a new *n*-alkane ratio, the GRIND index (for GRaminoid INDex), that computes as follows: (n-C_{27} + n-C_{33} + n-C_{35})/(n-C_{25} + n-C_{27} + n-C_{29} + n-C_{31} + n-C_{33} + n-C_{35}). This ratio may be used as an alternative to, or in combination with, $\delta^{13}C_{n\text{-alkane}}$ values to help resolve relative changes in C_3 and C_4 plant waxes, a proxy of the vegetation cover in the tropics.

By combining the $\delta^{13}C$ values of leaf wax *n*-alkanes from the CCB with existing $\delta^{13}C$ data from elsewhere in Africa, we have demonstrated that the occurrence of very negative $\delta^{13}C$ values in n-C_{29} and n-C_{31} alkanes (i.e., < –37‰), which are characteristic of C_3 plants, is almost exclusively limited to environments with high relative humidity. Applying these findings to sedimentary *n*-alkanes in peat and lake sediments may therefore help identify periods of RH > 80%, providing additional quantitative constraints for palaeo-climatic reconstructions.

The δD data from living plants in the CCB corroborates previous observations regarding the $\delta D_{n\text{-alkane}}$ values and the apparent fractionation (ε_{app}) between *n*-alkanes and the source water of the plants. This reveals significant disparities between C_3 and C_4 plants, as well as between dicots and monocots. These differences are mostly related to physiological variations in photosynthetic pathways and plant types.

Despite the potential presence of graminoids in humid equatorial areas, the strong dominance of C_3 and dicot plants at sampled sites heavily influences the sedimentary *n*-alkane characteristics. Major hydroclimate shifts — such as those seen in Africa during glacial-interglacial periods — can alter the dominant vegetation. In such cases, $\delta^{13}C_{n\text{-alkane}}$ data together with pollen data can help correct δD records, allowing for a clearer separation of climate signals from vegetation effects.

CRediT authorship contribution statement

Mélanie Guardiola: Writing – review & editing, Writing – original draft, Visualization, Validation, Methodology, Investigation, Formal analysis, Data curation, Conceptualization. **Gaël U.D. Bouka:** Writing – review & editing, Resources, Investigation. **Carolia Abaye:** Resources. **Johanna Menges:** Writing – review & editing, Resources. **Frauke Rostek:** Writing – review & editing, Resources, Methodology. **Guillaume Leduc:** Writing – review & editing, Resources. **Edouard Bard:** Writing – review & editing, Resources. **Enno Schefuß:** Writing – review & editing, Supervision, Resources, Project administration, Methodology, Funding acquisition, Conceptualization. **Yannick Garcin:** Writing – review & editing, Supervision, Resources, Project administration, Methodology, Funding acquisition, Conceptualization.

Declaration of competing interest

The authors declare that they have no known competing financial interests or personal relationships that could have appeared to influence the work reported in this paper.

Acknowledgments

This work was funded by the Agence Nationale de la Recherche (ANR, France) grant ANR-19-CE01-0022 to Yannick Garcin, and Deutsche Forschungsgemeinschaft (DFG, Germany) grant SCHE903/19-1 (project number 431458962) to Enno Schefuß (joint project 'ORACLE'). E. Schefuß was supported by the DFG–Cluster of Excellence 'The Ocean in the Earth System' at MARUM. We thank the Marien Ngouabi University in the Republic of the Congo for invaluable help and support and particularly Joël Loumeto. We thank the villages of Lobesi, Pasi Ya Kanda, Mokondo, and Botena who hosted our field campaigns. We thank Mackoul Koumba for field support and Élise Luciani at CEREGE for laboratory support. This study is a contribution to the IRD International Joint Laboratory 'Dynamics of land ecosystems in central Africa in a context of global changes' (LMI DYCOFAC). We thank Guillemette Ménot and Clément Duvert for fruitful discussions. We are grateful to Associate Editor Nikolai Pedentchouk, and Sarah Feakins and four anonymous reviewers, for their insightful comments and suggestions that strongly improved the quality of the initial manuscript.

Appendix A. Supplementary material

Supplementary data to this article can be found online at https://doi.org/10.1016/j.orggeochem.2025.105092.

Data availability

All data are available in Appendix A.

References

Alsdorf, D., Beighley, E., Laraque, A., Lee, H., Tshimanga, R., O'Loughlin, F., Mahé, G., Dinga, B., Moukandi, G., Spencer, R.G.M., 2016. Opportunities for hydrologic research in the Congo Basin. Reviews of Geophysics 54, 378–409. https://doi.org/10.1002/2016RG000517.

Badewien, T., Vogts, A., Rullkötter, J., 2015. *n*-Alkane distribution and carbon stable isotope composition in leaf waxes of C_3 and C_4 plants from Angola. Organic Geochemistry 89–90, 71–79. https://doi.org/10.1016/j.orggeochem.2015.09.002.

Bezabih, M., Pellikaan, W.F., Tolera, A., Hendriks, W.H., 2011. Evaluation of n-alkanes and their carbon isotope enrichments ($\delta^{13}C$) as diet composition markers. Animal 5, 57–66. https://doi.org/10.1017/S1751731110001515.

Bocquier, G., 1960. Caractérisation de quelques profils pédologiques observés dans le district de Souanke (République du Congo). ORSTOM-IEC, Paris.

Boissezon, P., Gras, F., 1970. Notice explicative. Carte pédologique Sibiti-Est, République du Congo Brazzaville à 1/500000. ORSTOM, Paris.

Bray, E.E., Evans, E.D., 1961. Distribution of *n*-paraffins as a clue to recognition of source beds. Geochimica et Cosmochimica Acta 22, 2–15. https://doi.org/10.1016/0016-7037(61)90069-2.

Bush, R.T., McInerney, F.A., 2013. Leaf wax *n*-alkane distributions in and across modern plants: implications for paleoecology and chemotaxonomy. Geochimica et Cosmochimica Acta 117, 161–179. https://doi.org/10.1016/j.gca.2013.04.016.

Campbell, D., 2005. The Congo River basin. In: Fraser, L.H., Keddy, P.A. (Eds.), The World's Largest Wetlands: Ecology and Conservation. Cambridge University Press, pp. 149–165.

Castañeda, I.S., Mulitza, S., Schefuß, E., Lopes Dos Santos, R.A., Sinninghe Damsté, J.S., Schouten, S., 2009. Wet phases in the Sahara/Sahel region and human migration patterns in North Africa. Proceedings of the National Academy of Sciences 106, 20159–20163. https://doi.org/10.1073/pnas.0905771106.

Chikaraishi, Y., Naraoka, H., 2003. Compound-specific δD–$\delta^{13}C$ analyses of *n*-alkanes extracted from terrestrial and aquatic plants. Phytochemistry 63, 361–371. https://doi.org/10.1016/S0031-9422(02)00749-5.

Collins, J.A., Schefuß, E., Heslop, D., Mulitza, S., Prange, M., Zabel, M., Tjallingii, R., Dokken, T.M., Huang, E., Mackensen, A., Schulz, M., Tian, J., Zarriess, M., Wefer, G., 2011. Interhemispheric symmetry of the tropical African rainbelt over the past 23,000 years. Nature Geoscience 4, 42–45. https://doi.org/10.1038/ngeo1039.

Collins, J.A., Schefuß, E., Mulitza, S., Prange, M., Werner, M., Tharammal, T., Paul, A., Wefer, G., 2013. Estimating the hydrogen isotopic composition of past precipitation using leaf-waxes from western Africa. Quaternary Science Reviews 65, 88–101. https://doi.org/10.1016/j.quascirev.2013.01.007.

Collister, J.W., Rieley, G., Stern, B., Eglinton, G., Fry, B., 1994. Compound-specific $\delta^{13}C$ analyses of leaf lipids from plants with differing carbon dioxide metabolisms. Organic Geochemistry 21, 619–627. https://doi.org/10.1016/0146-6380(94)90008-6.

Comptour, M., 2017. Entre pêche, agriculture et commerces, jouer avec la variabilité écologique et sociale: dynamique d'un système social-écologique dans les plaines inondables du fleuve Congo. Doctoral thesis. Université de Montpellier, France.

Comptour, M., Cosiaux, A., Coomes, O.T., Bader, J., Malaterre, P., Yoka, J., Caillon, S., McKey, D., 2020. Agricultural innovation and environmental change on the floodplains of the Congo River. The Geographical Journal 186, 16–30. https://doi.org/10.1111/geoj.12314.

Cranwell, P.A., 1984. Lipid geochemistry of sediments from Upton Broad, a small productive lake. Organic Geochemistry 7, 25–37. https://doi.org/10.1016/0146-6380(84)90134-7.

Crezee, B., Dargie, G.C., Ewango, C.E., Mitchard, E.T., Emba, B.O., Kanyama, T.J., Bola, P., Ndjango, J.B.N., Girkin, N.T., Bocko, Y.E., Ifo, S.A., Hubau, W., Seidensticker, D., Batumike, R., Imani, G., Cuní-Sanchez, A., Kiahtipes, C.A., Lebamba, J., Wotzka, H.-P., Bean, H., Baker, T.R., Baird, A.J., Boom, A., Morris, P.J., Page, S.E., Lawson, I.T., Lewis, S.L., 2022. Mapping peat thickness and carbon stocks of the central Congo Basin using field data. Nature Geoscience 15, 639–644. https://doi.org/10.1038/s41561-022-00966-7.

Dargie, G.C., Lawson, I.T., Rayden, T.J., Miles, L., Mitchard, E.T.A., Page, S.E., Bocko, Y. E., Ifo, S.A., Lewis, S.L., 2019. Congo Basin peatlands: threats and conservation priorities. Mitigation and Adaptation Strategies for Global Change 24, 669–686. https://doi.org/10.1007/s11027-017-9774-8.

Dargie, G.C., Lewis, S.L., Lawson, I.T., Mitchard, E.T.A., Page, S.E., Bocko, Y.E., Ifo, S.A., 2017. Age, extent and carbon storage of the central Congo Basin peatland complex. Nature 542, 86–90. https://doi.org/10.1038/nature21048.

Datok, P., Fabre, C., Sauvage, S., N'kaya, G.D.M., Paris, A., Dos Santos, V., Laraque, A., Sánchez-Pérez, J.-M., 2022. Investigating the role of the Cuvette Centrale in the hydrology of the Congo River Basin. In: Tshimanga, R.M., N'kaya, G.D.M., Alsdorf, D. (Eds.), Congo Basin Hydrology, Climate, and Biogeochemistry. Geophysical Monograph Series, AGU, pp. 247–273. https://doi.org/10.1002/9781119657002.ch14.

Davenport, I.J., McNicol, I., Mitchard, E.T.A., Dargie, G., Suspense, I., Milongo, B., Bocko, Y.E., Hawthorne, D., Lawson, I., Baird, A.J., Page, S., Lewis, S.L., 2020. First Evidence of Peat Domes in the Congo Basin using LiDAR from a Fixed-Wing Drone. Remote Sensing 12, 2196. https://doi.org/10.3390/rs12142196.

De Grandi, G.F., Mayaux, P., Rauste, Y., Rosenqvist, A., Simard, M., Saatchi, S., 2000. The Global Rain Forest Mapping Project JERS-1 radar mosaic of tropical Africa: development and product characterization aspects. IEEE Transaction on Geosciences and Remote Sensing 38, 2218–2233. https://doi.org/10.1109/36.868880.

Devred, R.F.E., 1958. La végétation forestière du Congo Belge et du Ruanda-Urundi. In: Bulletin de la Société Royale de Botanique de Belgique. 65, pp. 409–468.

Diefendorf, A.F., Freimuth, E.J., 2017. Extracting the most from terrestrial plant-derived *n*-alkyl lipids and their carbon isotopes from the sedimentary record: a review. Organic Geochemistry 103, 1–21. https://doi.org/10.1016/j.orggeochem.2016.10.016.

Doumenge, C., 1990. La conservation des écosystèmes forestiers du Zaïre. UICN, Gland, Suisse et Cambridge, Royaume-Uni, 242 p.

Duan, Y., He, J., 2011. Distribution and isotopic composition of *n*-alkanes from grass, reed and tree leaves along a latitudinal gradient in China. Geochemical Journal 45, 199–207. https://doi.org/10.2343/geochemj.1.0115.

Dyson, W.G., Herbin, G.A., 1968. Studies on plant cuticular waxes–IV: Leaf wax alkanes as a taxonomic discriminant for cypresses grown in Kenya. Phytochemistry 7, 1334–1344. https://doi.org/10.1016/S0031-9422(00)85634-4.

Eglinton, G., Hamilton, R.J., 1967. The waxy outer surfaces of most plants display a wide diversity of fine structure and chemical constituents. Geochimica et Cosmochimica Acta 170, 145–156. https://doi.org/10.1126/science.156.3780.1322.

Epstein, B.L., D'Hondt, S., Hargraves, P.E., 2001. The possible metabolic role of C_{37} alkenones in *Emiliania huxleyi*. Organic Geochemistry 32, 867–875. https://doi.org/10.1016/S0146-6380(01)00026-2.

Evrard, C., 1968. Recherches écologiques sur le peuplement forestier des sols hydromorphes de la Cuvette centrale congolaise. Publications de l'Institut national pour l'étude agronomique du Congo, Série Scientifique 110, Bruxelles.

Farquhar, G., O'Leary, M., Berry, J., 1982. On the relationship between carbon isotope discrimination and the intercellular carbon dioxide concentration in leaves. Functional Plant Biology 9, 121. https://doi.org/10.1071/PP9820121.

Farquhar, G.D., Ehleringer, J.R., Hubick, K.T., 1989. Carbon isotope discrimination and photosynthesis. Annual Review of Plant Physiology and Plant Molecular Biology 40, 503–537. https://doi.org/10.1146/annurev.pp.40.060189.002443.

Feakins, S.J., 2013. Pollen-corrected leaf wax D/H reconstructions of northeast African hydrological changes during the late Miocene. Palaeogeography, Palaeoclimatology, Palaeoecology 374, 62–71. https://doi.org/10.1016/j.palaeo.2013.01.004.

Feakins, S.J., deMenocal, P.B., Eglinton, T.I., 2005. Biomarker records of late Neogene changes in northeast African vegetation. Geology 33, 977. https://doi.org/10.1130/G21814.1.

Feakins, S.J., Sessions, A.L., 2010. Controls on the D/H ratios of plant leaf waxes in an arid ecosystem. Geochimica et Cosmochimica Acta 74, 2128–2141. https://doi.org/10.1016/j.gca.2010.01.016.

Francey, R.J., Allison, C.E., Etheridge, D.M., Trudinger, C.M., Enting, I.G., Leuenberger, M., Langenfelds, R.L., Michel, E., Steele, L.P., 1999. A 1000-year high precision record of $\delta^{13}C$ in atmospheric CO_2. Tellus B 51, 170–193. https://doi.org/10.1034/j.1600-0889.1999.t01-1-00005.x.

Garcin, Y., Deschamps, P., Ménot, G., de Saulieu, G., Schefuß, E., Sebag, D., Dupont, L.M., Oslisly, R., Brademann, B., Mbusnum, K.G., Onana, J.-M., Ako, A.A., Epp, L.S., Tjallingii, R., Strecker, M.R., Brauer, A., Sachse, D., 2018. Early anthropogenic impact on Western Central African rainforests 2,600 y ago. Proceedings of the National Academy of Sciences 115, 3261–3266. https://doi.org/10.1073/pnas.1715336115.

Garcin, Y., Schefuß, E., Dargie, G.C., Hawthorne, D., Lawson, I.T., Sebag, D., Biddulph, G. E., Crezee, B., Bocko, Y.E., Ifo, S.A., Mampouya Wenina, Y.E., Mbemba, M., Ewango, C.E.N., Emba, O., Bola, P., Kanyama Tabu, J., Tyrrell, G., Young, D.M., Gassier, G., Girkin, N.T., Vane, C.H., Adatte, T., Baird, A.J., Boom, A., Gulliver, P., Morris, P.J., Page, S.E., Sjögersten, S., Lewis, S.L., 2022. Hydroclimatic vulnerability of peat carbon in the central Congo Basin. Nature 612, 277–282. https://doi.org/10.1038/s41586-022-05389-3.

Garcin, Y., Schefuß, E., Schwab, V.F., Garreta, V., Gleixner, G., Vincens, A., Todou, G., Séné, O., Onana, J.-M., Achoundong, G., Sachse, D., 2014. Reconstructing C_3 and C_4 vegetation cover using *n*-alkane carbon isotope ratios in recent lake sediments from Cameroon, Western Central Africa. Geochimica et Cosmochimica Acta 142, 482–500. https://doi.org/10.1016/j.gca.2014.07.004.

Garcin, Y., Schwab, V.F., Gleixner, G., Kahmen, A., Todou, G., Séné, O., Onana, J.-M., Achoundong, G., Sachse, D., 2012. Hydrogen isotope ratios of lacustrine sedimentary *n*-alkanes as proxies of tropical African hydrology: Insights from a calibration transect across Cameroon. Geochimica et Cosmochimica Acta 79, 106–126. https://doi.org/10.1016/j.gca.2011.11.039.

Gaviria-Lugo, N., Läuchli, C., Wittmann, H., Bernhardt, A., Frings, P., Mohtadi, M., Rach, O., Sachse, D., 2023. Climatic controls on leaf wax hydrogen isotope ratios in terrestrial and marine sediments along a hyperarid-to-humid gradient. Biogeosciences 20, 4433–4453. https://doi.org/10.5194/bg-20-4433-2023.

Gensel, J., Humphries, M.S., Zabel, M., Sebag, D., Hahn, A., Schefuß, E., 2022. Origin, transport, and retention of fluvial sedimentary organic matter in South Africa's largest freshwater wetland, Mkhuze Wetland System. Biogeosciences 19, 2881–2902. https://doi.org/10.5194/bg-19-2881-2022.

Gérard, P., 1960. Etude Ecologique de la Forêt Dense à *Gilbertiodendron Dewevrei* dans la Région de l'Uele. Publications de l'Institut national pour l'étude agronomique du Congo, Série Scientifique 87, Bruxelles.

Gilbert, G., 1984. La masse forestière congolaise. Son implantation, ses divers faciès. Bois & Forêts des Tropiques 204, 3–19. https://doi.org/10.19182/bft1984.204.a19505.

Graham, H.V., Patzkowsky, M.E., Wing, S.L., Parker, G.G., Fogel, M.L., Freeman, K.H., 2014. Isotopic characteristics of canopies in simulated leaf assemblages. Geochimica et Cosmochimica Acta 144, 82–95. https://doi.org/10.1016/j.gca.2014.08.032.

Grantham, H.S., Duncan, A., Evans, T.D., Jones, K.R., Beyer, H.L., Schuster, R., Walston, J., Ray, J.C., Robinson, J.G., Callow, M., Clements, T., Costa, H.M., DeGemmis, A., Elsen, P.R., Ervin, J., Franco, P., Goldman, E., Goetz, S., Hansen, A., Hofsvang, E., Jantz, P., Jupiter, S., Kang, A., Langhammer, P., Laurance, W.F., Lieberman, S., Linkie, M., Malhi, Y., Maxwell, S., Mendez, M., Mittermeier, R., Murray, N.J., Possingham, H., Radachowsky, J., Saatchi, S., Samper, C., Silverman, J., Shapiro, A., Strassburg, B., Stevens, T., Stokes, E., Taylor, R., Tear, T., Tizard, R., Venter, O., Visconti, P., Wang, S., Watson, J.E.M., 2020. Anthropogenic modification of forests means only 40% of remaining forests have high ecosystem integrity. Nature Communications 11, 5978. https://doi.org/10.1038/s41467-020-19493-3.

Griepentrog, M., De Wispelaere, L., Bauters, M., Bodé, S., Hemp, A., Verschuren, D., Boeckx, P., 2019. Influence of plant growth form, habitat and season on leaf-wax *n*-alkane hydrogen-isotopic signatures in equatorial East Africa. Geochimica et Cosmochimica Acta 263, 122–139. https://doi.org/10.1016/j.gca.2019.08.004.

Hansen, M.C., Roy, D.P., Lindquist, E., Adusei, B., Justice, C.O., Altstatt, A., 2008. A method for integrating MODIS and Landsat data for systematic monitoring of forest cover and change in the Congo Basin. Remote Sensing of Environment 112, 2495–2513. https://doi.org/10.1016/j.rse.2007.11.012.

Hawthorne, D., Lawson, I.T., Dargie, G.C., Bocko, Y.E., Ifo, S.A., Garcin, Y., Schefuß, E., Hiles, W., Jovani-Sancho, A.J., Tyrrell, G., Biddulph, G.E., Boom, A., Chase, B.M., Gulliver, P., Page, S.E., Roucoux, K.H., Sjögersten, S., Young, D.M., Lewis, S.L., 2023. Genesis and development of an interfluvial peatland in the central Congo Basin since the Late Pleistocene. Quaternary Science Reviews 305, 107992. https://doi.org/10.1016/j.quascirev.2023.107992.

Hersbach, H., Bell, B., Berrisford, P., Hirahara, S., Horányi, A., Muñoz-Sabater, J., Nicolas, J., Peubey, C., Radu, R., Schepers, D., Simmons, A., Soci, C., Abdalla, S., Abellan, X., Balsamo, G., Bechtold, P., Biavati, G., Bidlot, J., Bonavita, M., De Chiara, G., Dahlgren, P., Dee, D., Diamantakis, M., Dragani, R., Flemming, J., Forbes, R., Fuentes, M., Geer, A., Haimberger, L., Healy, S., Hogan, R.J., Hólm, E., Janisková, M., Keeley, S., Laloyaux, P., Lopez, P., Lupu, C., Radnoti, G., De Rosnay, P., Rozum, I., Vamborg, F., Villaume, S., Thépaut, J., 2020. The ERA5 global reanalysis. Quarterly Journal of the Royal Meteorological Society 146, 1999–2049. https://doi.org/10.1002/qj.3803.

Hoffmann, B., Kahmen, A., Cernusak, L.A., Arndt, S.K., Sachse, D., 2013. Abundance and distribution of leaf wax *n*-alkanes in leaves of Acacia and Eucalyptus trees along a strong humidity gradient in northern Australia. Organic Geochemistry 62, 62–67. https://doi.org/10.1016/j.orggeochem.2013.07.003.

Holmes, M.E., Chanton, J.P., Tfaily, M.M., Ogram, A., 2015. CO_2 and CH_4 isotope compositions and production pathways in a tropical peatland. Global Biogeochemical Cycles 29, 1–18. https://doi.org/10.1002/2014GB004951.

Hugues, R.H., Hugues, J.S., 1992. A directory of African wetlands. IUCN, Gland, Switzerland and Cambridge, UK, UNEP, Nairobi, Kenya, WCMC, Cambridge, UK, 820 p.

IAEA/WMO, 2020. Global Network of Isotopes in Precipitation: The GNIP Database. International Atomic Energy Agency/World Meteorological Organization, Vienna. https://www.iaea.org/services/networks/gnip.

Ifo, S.A., Moutsambote, J.-M., Koubouana, F., Yoka, J., Ndzai, S.F., Bouetou-Kadilamio, L.N.O., Mampouya, H., Jourdain, C., Bocko, Y., Mantota, A.B., Mbemba, M., Mouanga-Sokath, D., Odende, R., Mondzali, L.R., Wenina, Y.E.M., Ouissika, B.C., Joel, L.J., 2016. Tree species diversity, richness, and similarity in intact and degraded forest in the tropical rainforest of the Congo Basin: case of the forest of Likouala in the Republic of Congo. International Journal of Forestry Research 2016, 1–12. https://doi.org/10.1155/2016/7593681.

Jaeschke, A., Thienemann, M., Schefuß, E., Urban, J., Schäbitz, F., Wagner, B., Rethemeyer, J., 2020. Holocene Hydroclimate Variability and Vegetation Response

in the Ethiopian Highlands (Lake Dendi). Frontiers in Earth Science 8. https://doi.org/10.3389/feart.2020.585770.
Kahmen, A., Dawson, T.E., Vieth, A., Sachse, D., 2011. Leaf wax *n*-alkane δD values are determined early in the ontogeny of Populus trichocarpa leaves when grown under controlled environmental conditions. Plant, Cell & Environment 34, 1639–1651. https://doi.org/10.1111/j.1365-3040.2011.02360.x.
Kahmen, A., Schefuß, E., Sachse, D., 2013. Leaf water deuterium enrichment shapes leaf wax *n*-alkane δD values of angiosperm plants I: Experimental evidence and mechanistic insights. Geochimica et Cosmochimica Acta 111, 39–49. https://doi.org/10.1016/j.gca.2012.09.003.
Kassambara, A., 2023. rstatix: Pipe-Friendly Framework for Basic Statistical Tests. R packageversion 0.7.2. https://CRAN.R-project.org/package=rstatix.
Keddy, P.A., Fraser, L.H., Solomeshch, A.I., Junk, W.J., Campbell, D.R., Arroyo, M.T.K., Alho, C.J.R., 2009. Wet and wonderful: the world's largest wetlands are conservation priorities. Bioscience 59, 39–51. https://doi.org/10.1525/bio.2009.59.1.8.
Keeling, R.F., Piper, S.C., Bollenbacher, A.F., Walker, S.J., 2018. Monthly Atmospheric $^{13}C/^{12}C$ Isotopic Ratios for 11 SIO Stations (1977-2008). ESS-DIVE. https://doi.org/10.3334/CDIAC/ATG.025.
Koechlin, J., 1961. La Végétation des Savanes dans le Sud de la République du Congo. ORSTOM, Montpellier.
Kristen, I., Wilkes, H., Vieth, A., Zink, K.-G., Plessen, B., Thorpe, J., Partridge, T.C., Oberhänsli, H., 2010. Biomarker and stable carbon isotope analyses of sedimentary organic matter from Lake Tswaing: evidence for deglacial wetness and early Holocene drought from South Africa. Journal of Paleolimnology 44, 143–160. https://doi.org/10.1007/s10933-009-9393-9.
Krull, E., Sachse, D., Mügler, I., Thiele, A., Gleixner, G., 2006. Compound-specific $\delta^{13}C$ and $\delta^{2}H$ analyses of plant and soil organic matter: A preliminary assessment of the effects of vegetation change on ecosystem hydrology. Soil Biology and Biochemistry 38, 3211–3221. https://doi.org/10.1016/j.soilbio.2006.04.008.
Ladd, S.N., Maloney, A.E., Nelson, D.B., Prebble, M., Camperio, G., Sear, D.A., Hassall, J. D., Langdon, P.G., Sachs, J.P., Dubois, N., 2021. Leaf Wax Hydrogen Isotopes as a Hydroclimate Proxy in the Tropical Pacific. Journal of Geophysical Research: Biogeosciences 126, e2020JG005891. https://doi.org/10.1029/2020JG005891.
Laidet, D., 1969. Carte géologique de la république du Congo : planche VIII, Atlas du Congo. Service cartographique de l'ORSTOM, Paris.
Laporte, N.T., Goetz, S.J., Justice, C.O., Heinicke, M., 1998. A new land cover map of central Africa derived from multi-resolution, multi-temporal AVHRR data. International Journal of Remote Sensing 19, 3537–3550. https://doi.org/10.1080/014311698213803.
Laraque, A., Bricquet, J.P., Pandi, A., Olivry, J.C., 2009. A review of material transport by the Congo River and its tributaries. Hydrological Processes 23, 3216–3224. https://doi.org/10.1002/hyp.7395.
Laraque, A., Moukandi N'kaya, G.D., Orange, D., Tshimanga, R., Tshitenge, J.M., Mahé, G., Nguimalet, C.R., Trigg, M.A., Yepez, S., Gulemvuga, G., 2020. Recent Budget of Hydroclimatology and Hydrosedimentology of the Congo River in Central Africa. Water 12, 2613. https://doi.org/10.3390/w12092613.
Laraque, A., Olivry, J.C., 1996. Evolution de l'hydrologie du Congo-Zaïre et de ses affluents rive droite et dynamique des transports solides et dissous. in: L'Hydrologie Tropicale: Géoscience et Outil Pour Le Développement. IAHS Press, Wallingford, U. K., pp. 271–288
Lebrun, J., Gilbert, G., 1954. Une classification écologique des forêts du Congo, in: Série Scientifique. Bruxelles, p. 89.
Lebrun, J.-P., Stork, A.L., 2020. Tropical African flowering plants: Ecology and distribution, Cyperaceae, 11. Éditions des Conservatoire et Jardin Botaniques, Genève, Switzerland.
Lee, H., Yuan, T., Jung, H.C., Beighley, E., 2015. Mapping wetland water depths over the central Congo Basin using PALSAR ScanSAR, Envisat altimetry, and MODIS VCF data. Remote Sensing of Environment 159, 70–79. https://doi.org/10.1016/j.rse.2014.11.030.
Lewis, S.L., Sonké, B., Sunderland, T., Begne, S.K., Lopez-Gonzalez, G., Van Der Heijden, G.M.F., Phillips, O.L., Affum-Baffoe, K., Baker, T.R., Banin, L., Bastin, J.-F., Beeckman, H., Boeckx, P., Bogaert, J., De Cannière, C., Chezeaux, E., Clark, C.J., Collins, M., Djagbletey, G., Djuikouo, M.N.K., Droissart, V., Doucet, J.-L., Ewango, C. E.N., Fauset, S., Feldpausch, T.R., Foli, E.G., Gillet, J.-F., Hamilton, A.C., Harris, D.J., Hart, T.B., De Haulleville, T., Hladik, A., Hufkens, K., Huygens, D., Jeanmart, P., Jeffery, K.J., Kearsley, E., Leal, M.E., Lloyd, J., Lovett, J.C., Makana, J.-R., Malhi, Y., Marshall, A.R., Ojo, L., Peh, K.-S.-H., Pickavance, G., Poulsen, J.R., Reitsma, J.M., Sheil, D., Simo, M., Steppe, K., Taedoumg, H.E., Talbot, J., Taplin, J.R.D., Taylor, D., Thomas, S.C., Toirambe, B., Verbeeck, H., Vleminckx, J., White, L.J.T., Willcock, S., Woell, H., Zemagho, L., 2013. Above-ground biomass and structure of 260 African tropical forests. Philosophical Transactions of the Royal Society b: Biological Sciences 368, 20120295. https://doi.org/10.1098/rstb.2012.0295.
Liu, H., Wang, S., Wang, H., Cao, Y., Hu, J., Liu, W., 2023. Apparent fractionation of hydrogen isotope from precipitation to leaf wax *n*-alkanes from natural environments and manipulation experiments. Science of the Total Environment 877, 162970. https://doi.org/10.1016/j.scitotenv.2023.162970.
Liu, J., An, Z., Liu, H., 2018. Leaf wax *n*-alkane distributions across plant types in the central Chinese Loess Plateau. Organic Geochemistry 125, 260–269. https://doi.org/10.1016/j.orggeochem.2018.09.006.
Liu, J., Zhao, J., He, D., Huang, X., Jiang, C., Yan, H., Lin, G., An, Z., 2022. Effects of plant types on terrestrial leaf wax long-chain *n*-alkane biomarkers: implications and paleoapplications. Earth-Science Reviews 235, 104248. https://doi.org/10.1016/j.earscirev.2022.104248.
Lockheart, M.J., Van Bergen, P.F., Evershed, R.P., 1997. Variations in the stable carbon isotope compositions of individual lipids from the leaves of modern angiosperms: implications for the study of higher land plant-derived sedimentary organic matter. Organic Geochemistry 26, 137–153. https://doi.org/10.1016/S0146-6380(96)00135-0.
Madhavan, S., Treichel, I., O'Leary, M.H., 1991. Effects of relative humidity on carbon isotope fractionation in plants. Botanica Acta 104, 292–294. https://doi.org/10.1111/j.1438-8677.1991.tb00232.x.
Mayaux, P., Grandi, G.D., Malingreau, J.-P., 2000. Central African forest cover revisited: a multisatellite analysis. Remote Sensing of Environment 71, 183–196. https://doi.org/10.1016/S0034-4257(99)00073-5.
McCarroll, D., Loader, N.J., 2004. Stable isotopes in tree rings. Quaternary Science Reviews 23, 771–801. https://doi.org/10.1016/j.quascirev.2003.06.017.
Menges, J., Sebag, D., Lebamba, J., Kiahtipes, C., Wotzka, H.-P., Preuß, J., Bwamangele, F.B., Lutonadio, R.K., Guardiola, M., Adatte, T., Stroobandt, Y., Bouillon, S., Garcin, Y., Schefuß, E., 2025. Environmental and climatic evolution of a river-proximal peatland in the Cuvette Centrale, Congo Basin. Quaternary Science Reviews 363, 109445. https://doi.org/10.1016/j.quascirev.2025.109445.
Meyers, P.A., 1997. Organic geochemical proxies of paleoceanographic, paleolimnologic, and paleoclimatic processes. Organic Geochemistry 27, 213–250. https://doi.org/10.1016/S0146-6380(97)00049-1.
Meyers, P.A., 2003. Applications of organic geochemistry to paleolimnological reconstructions: a summary of examples from the Laurentian Great Lakes. Organic Geochemistry 34, 261–289. https://doi.org/10.1016/S0146-6380(02)00168-7.
Molinario, G., Hansen, M.C., Potapov, P.V., 2015. Forest cover dynamics of shifting cultivation in the Democratic Republic of Congo: a remote sensing-based assessment for 2000–2010. Environmental Research Letters 10, 094009. https://doi.org/10.1088/1748-9326/10/9/094009.
Molinario, G., Hansen, M.C., Potapov, P.V., Tyukavina, A., Stehman, S., Barker, B., Humber, M., 2017. Quantification of land cover and land use within the rural complex of the Democratic Republic of Congo. Environmental Research Letters 12, 104001. https://doi.org/10.1088/1748-9326/aa8680.
Moutsambote, J.-M., 2012. Étude écologique, phytogéographique et phytosociologique du Congo septentrional (Plateaux, Cuvettes, Likouala et Sangha). Thèse de doctorat. Université Marien Ngouabi, Brazzaville, République du Congo.
Niedermeyer, E.M., Schefuß, E., Sessions, A.L., Mulitza, S., Mollenhauer, G., Schulz, M., Wefer, G., 2010. Orbital- and millennial-scale changes in the hydrologic cycle and vegetation in the western African Sahel: insights from individual plant wax δD and $\delta^{13}C$. Quaternary Science Reviews 29, 2996–3005. https://doi.org/10.1016/j.quascirev.2010.06.039.
Page, S.E., Rieley, J.O., Banks, C.J., 2011. Global and regional importance of the tropical peatland carbon pool. Global Change Biology 17, 798–818. https://doi.org/10.1111/j.1365-2486.2010.02279.x.
Pancost, R.D., 2024. Biomarker carbon and hydrogen isotopes reveal changing peatland vegetation, hydroclimate and biogeochemical tipping points. Quaternary Science Reviews 339, 108828. https://doi.org/10.1016/j.quascirev.2024.108828.
Pancost, R.D., Boot, C.S., 2004. The palaeoclimatic utility of terrestrial biomarkers in marine sediments. Marine Chemistry 92, 239–261. https://doi.org/10.1016/j.marchem.2004.06.029.
Pedentchouk, N., Sumner, W., Tipple, B., Pagani, M., 2008. $\delta^{13}C$ and δD compositions of *n*-alkanes from modern angiosperms and conifers: an experimental set up in central Washington State, USA. Organic Geochemistry 39, 1066–1071. https://doi.org/10.1016/j.orggeochem.2008.02.005.
Peeters, L., 1964. Les limites forêt-savane dans le nord du Congo en relation avec le milieu géographique, CEMUBAC. ed. Bruxelles.
Poynter, J.G., Farrimond, P., Robinson, N., Eglinton, G., 1989. Aeolian-derived higher plant lipids in the marine sedimentary records: links with paleoclimate. In: Leinen, M., Sarnthein, M. (Eds.), Paleoclimatology and Paleometeorology: Modern and Past Patterns of Global Atmospheric Transport. Kluwer Academic, Norwell, MA, pp. 435–462.
R Core Team, 2022. R: A Language and Environment for Statistical Computing.
Raghoebarsing, A.A., Smolders, A.J.P., Schmid, M.C., Rijpstra, W.I.C., Wolters-Arts, M., Derksen, J., Jetten, M.S.M., Schouten, S., Sinninghe Damsté, J.S., Lamers, L.P.M., Roelofs, J.G.M., Op Den Camp, H.J.M., Strous, M., 2005. Methanotrophic symbionts provide carbon for photosynthesis in peat bogs. Nature 436, 1153–1156. https://doi.org/10.1038/nature03802.
Rieley, G., Collier, R.J., Jones, D.M., Eglinton, G., 1991. The biogeochemistry of Ellesmere Lake, U.K.—I: source correlation of leaf wax inputs to the sedimentary lipid record. Organic Geochemistry 17, 901–912. https://doi.org/10.1016/0146-6380(91)90031-E.
Rommerskirchen, F., Eglinton, G., Dupont, L., Güntner, U., Wenzel, C., Rullkötter, J., 2003. A north to south transect of Holocene southeast Atlantic continental margin sediments: Relationship between aerosol transport and compound-specific $\delta^{13}C$ land plant biomarker and pollen records. Geochemistry, Geophysics, Geosystems 4, 2003GC000541. https://doi.org/10.1029/2003GC000541.
Rommerskirchen, F., Plader, A., Eglinton, G., Chikaraishi, Y., Rullkötter, J., 2006. Chemotaxonomic significance of distribution and stable carbon isotopic composition of long-chain alkanes and alkan-1-ols in C_4 grass waxes. Organic Geochemistry 37, 1303–1332. https://doi.org/10.1016/j.orggeochem.2005.12.013.
Sachse, D., Billault, I., Bowen, G.J., Chikaraishi, Y., Dawson, T.E., Feakins, S.J., Freeman, K.H., Magill, C.R., McInerney, F.A., Van Der Meer, M.T.J., Polissar, P., Robins, R.J., Sachs, J.P., Schmidt, H.-L., Sessions, A.L., White, J.W.C., West, J.B., Kahmen, A., 2012. Molecular paleohydrology: interpreting the hydrogen-isotopic composition of lipid biomarkers from photosynthesizing organisms. Annual Review of Earth and Planetary Sciences 40, 221–249. https://doi.org/10.1146/annurev-earth-042711-105535.
Sachse, D., Radke, J., Gleixner, G., 2006. δD values of individual *n*-alkanes from terrestrial plants along a climatic gradient – Implications for the sedimentary

biomarker record. Organic Geochemistry 37, 469–483. https://doi.org/10.1016/j.orggeochem.2005.12.003.
Samba, G., Toli, G., Poadzola Ngomboho, P., 2023. Vulnérabilité aux changements climatiques des marges occidentales du bassin du Congo dans les zones Ollombo, Oyo et Owando. Les Cahiers de l'IGRAC 24, 99–127.
Sankaran, M., Hanan, N.P., Scholes, R.J., Ratnam, J., Augustine, D.J., Cade, B.S., Gignoux, J., Higgins, S.I., Le Roux, X., Ludwig, F., Ardo, J., Banyikwa, F., Bronn, A., Bucini, G., Caylor, K.K., Coughenour, M.B., Diouf, A., Ekaya, W., Feral, C.J., February, E.C., Frost, P.G.H., Hiernaux, P., Hrabar, H., Metzger, K.L., Prins, H.H.T., Ringrose, S., Sea, W., Tews, J., Worden, J., Zambatis, N., 2005. Determinants of woody cover in African savannas. Nature 438, 846–849. https://doi.org/10.1038/nature04070.
Schefuß, E., Kuhlmann, H., Mollenhauer, G., Prange, M., 2011. Forcing of south-east African wet phases during the last 17,000 years. Nature 480, 509–512. https://doi.org/10.1038/nature10685.
Schefuß, E., Ratmeyer, V., Stuut, J.-B.-W., Jansen, J.H.F., Sinninghe Damsté, J.S., 2003. Carbon isotope analyses of *n*-alkanes in dust from the lower atmosphere over the central eastern Atlantic. Geochimica et Cosmochimica Acta 67, 1757–1767. https://doi.org/10.1016/S0016-7037(02)01414-X.
Schefuß, E., Schouten, S., Schneider, R.R., 2005. Climatic controls on central African hydrology during the past 20,000 years. Nature 437, 1003–1006. https://doi.org/10.1038/nature03945.
Schimmelmann, A., Lewan, M.D., Wintsch, R.P., 1999. D/H isotope ratios of kerogen, bitumen, oil, and water in hydrous pyrolysis of source rocks containing kerogen types I, II, IIS, and III. Geochimica et Cosmochimica Acta 63, 3751–3766. https://doi.org/10.1016/S0016-7037(99)00221-5.
Seki, O., Nakatsuka, T., Shibata, H., Kawamura, K., 2010. A compound-specific *n*-alkane $\delta^{13}C$ and δD approach for assessing source and delivery processes of terrestrial organic matter within a forested watershed in northern Japan. Geochimica et Cosmochimica Acta 74, 599–613. https://doi.org/10.1016/j.gca.2009.10.025.
Sessions, A.L., 2016. Factors controlling the deuterium contents of sedimentary hydrocarbons. Organic Geochemistry 96, 43–64. https://doi.org/10.1016/j.orggeochem.2016.02.012.
Shanahan, T.M., McKay, N.P., Hughen, K.A., Overpeck, J.T., Otto-Bliesner, B., Heil, C.W., King, J., Scholz, C.A., Peck, J., 2015. The time-transgressive termination of the African Humid Period. Nature Geoscience 8, 140–144. https://doi.org/10.1038/ngeo2329.
Shapiro, A., d'Annunzio, R., Desclée, B., Jungers, Q., Kondjo, H.K., Iyanga, J.M., Gangyo, F.I., Nana, T., Obame, C.V., Milandou, C., Rambaud, P., Sonwa, D.J., Mertens, B., Tchana, E., Khasa, D., Bourgoin, C., Ouissika, C.B., Kipute, D.D., 2023. Small scale agriculture continues to drive deforestation and degradation in fragmented forests in the Congo Basin (2015–2020). Land Use Policy 134, 106922. https://doi.org/10.1016/j.landusepol.2023.106922.
Shapiro, A.C., Grantham, H.S., Aguilar-Amuchastegui, N., Murray, N.J., Gond, V., Bonfils, D., Rickenbach, O., 2021. Forest condition in the Congo Basin for the assessment of ecosystem conservation status. Ecological Indicators 122, 107268. https://doi.org/10.1016/j.ecolind.2020.107268.
Smith, F.A., Freeman, K.H., 2006. Influence of physiology and climate on δD of leaf wax *n*-alkanes from C_3 and C_4 grasses. Geochimica et Cosmochimica Acta 70, 1172–1187. https://doi.org/10.1016/j.gca.2005.11.006.
Tierney, J.E., Pausata, F.S.R., deMenocal, P.B., 2017. Rainfall regimes of the Green Sahara. Science Advances 3, e1601503. https://doi.org/10.1126/sciadv.1601503.
Tierney, J.E., Russell, J.M., Huang, Y., 2010. A molecular perspective on Late Quaternary climate and vegetation change in the Lake Tanganyika basin, East Africa. Quaternary Science Reviews 29, 787–800. https://doi.org/10.1016/j.quascirev.2009.11.030.
Tipple, B.J., Pagani, M., 2013. Environmental control on eastern broadleaf forest species' leaf wax distributions and D/H ratios. Geochimica et Cosmochimica Acta 111, 64–77. https://doi.org/10.1016/j.gca.2012.10.042.
Trochain, J.L., 1957. Accord interafricain sur la définition des types de végétation de l'Afrique tropicale. Bulletin de l'Institut d'Etudes Centrafricaine 13–14 55–93.
Tweedy, R.R., Strömberg, C., Reichgelt, T., Kinyanjui, R.N., Kimeu, M., Munyaka, V., Uno, K.T., 2025. African C_3 grass *n*-alkane distributions & plant chemotaxonomy. Organic Geochemistry 104994. https://doi.org/10.1016/j.orggeochem.2025.104994.
Van Der Merwe, N.J., Medina, E., 1991. The canopy effect, carbon isotope ratios and foodwebs in amazonia. Journal of Archaeological Science 18, 249–259. https://doi.org/10.1016/0305-4403(91)90064-V.
Van Winden, J.F., Talbot, H.M., Reichart, G., McNamara, N.P., Benthien, A., Sinninghe Damsté, J.S., 2020. Influence of temperature on the $\delta^{13}C$ values and distribution of methanotroph-related hopanoids in Sphagnum-dominated peat bogs. Geobiology 18, 497–507. https://doi.org/10.1111/gbi.12389.
Vennetier, P., 1966. Géographie du Congo-Brazzaville. In: Enseignement supérieur en Afrique centrale. Gauthier-Villars, Paris.
Verhegghen, A., Mayaux, P., De Wasseige, C., Defourny, P., 2012. Mapping Congo Basin vegetation types from 300 m and 1 km multi-sensor time series for carbon stocks and forest areas estimation. Biogeosciences 9, 5061–5079. https://doi.org/10.5194/bg-9-5061-2012.
Vogts, A., Moossen, H., Rommerskirchen, F., Rullkötter, J., 2009. Distribution patterns and stable carbon isotopic composition of alkanes and alkan-1-ols from plant waxes of African rain forest and savanna C_3 species. Organic Geochemistry 40, 1037–1054. https://doi.org/10.1016/j.orggeochem.2009.07.011.
Wang, J., Axia, E., Xu, Y., Wang, G., Zhou, L., Jia, Y., Chen, Z., Li, J., 2018. Temperature effect on abundance and distribution of leaf wax *n*-alkanes across a temperature gradient along the 400 mm isohyet in China. Organic Geochemistry 120, 31–41. https://doi.org/10.1016/j.orggeochem.2018.03.009.
Wang, Y.V., Larsen, T., Leduc, G., Andersen, N., Blanz, T., Schneider, R.R., 2013. What does leaf wax δD from a mixed C_3/C_4 vegetation region tell us? Geochimica et Cosmochimica Acta 111, 128–139. https://doi.org/10.1016/j.gca.2012.10.016.
White, F., 1983. The Vegetation of Africa: A Descriptive Memoir to Accompany the UNESCO/AETFAT/UNSO Vegetation Map of Africa. UNESCO, Paris.
Winter, K., 1981. CO_2 and Water Vapour Exchange, Malate Content and $\delta^{13}C$ Value in *Cicer arietinum*. Zeitschrift Für Pflanzenphysiologie 101, 421–430. https://doi.org/10.1016/S0044-328X(81)80081-5.
Wongchuig, S., Kitambo, B., Papa, F., Paris, A., Fleischmann, A.S., Gal, L., Boucharel, J., Paiva, R., Oliveira, R.J., Tshimanga, R.M., Calmant, S., 2023. Improved modeling of Congo's hydrology for floods and droughts analysis and ENSO teleconnections. Journal of Hydrology: Regional Studies 50, 101563. https://doi.org/10.1016/j.ejrh.2023.101563.
Wu, M.S., Feakins, S.J., Martin, R.E., Shenkin, A., Bentley, L.P., Blonder, B., Salinas, N., Asner, G.P., Malhi, Y., 2017. Altitude effect on leaf wax carbon isotopic composition in humid tropical forests. Geochimica et Cosmochimica Acta 206, 1–17. https://doi.org/10.1016/j.gca.2017.02.022.
Yang, D., Bowen, G.J., 2022. Integrating plant wax abundance and isotopes for paleovegetation and paleoclimate reconstructions: a multi-source mixing model using a Bayesian framework. Climate of the past 18, 2181–2210. https://doi.org/10.5194/cp-18-2181-2022.
Zhang, H., Yang, M., Zhang, W., Lei, G., Chang, F., Pu, Y., Fan, H., 2008. Molecular fossil and paleovegetation records of paleosol S4 and adjacent loess layers in the Luochuan loess section, NW China. Science in China Series d: Earth Sciences 51, 321–330. https://doi.org/10.1007/s11430-008-0012-9.
Zhao, B., Russell, J.M., Blaus, A., Nascimento, M.D.N., Freeman, A., Bush, M.B., 2024. Tropical Andean climate variations since the last deglaciation. Proceedings of the National Academy of Sciences 121, e2320143121. https://doi.org/10.1073/pnas.2320143121.